CLM-P746

CLM-P746

UKAEA

Preprint

ATOMIC AND MOLECULAR COLLISIONS IN THE PLASMA BOUNDARY

M. F. A. HARRISON

CULHAM LABORATORY
Abingdon, Oxfordshire

January 1985

CLM-P 746

ATOMIC AND MOLECULAR COLLISIONS IN THE PLASMA BOUNDARY

M.F.A. Harrison

UKAEA/Euratom Fusion Association
Culham Laboratory, Abingdon, Oxon OX14 3DB, England

A series of lectures presented at the NATO
Advanced Study Institute, Val-Morin, Canada,
30th July - 10th August, 1984.

ABSTRACT

The objective of this paper is to provide an introduction to those aspects of atomic collision physics which underly the unavoidably generalised base of cross section data and scaling relationships which is currently employed in plasma modelling. Both experimental and theoretical methods are outlined and, where practicable, general trends in collisional behaviour are illustrated by examples of measured data. Atomic and molecular processes are considered on the basis of their particular relevance to the plasma edge region so that the discussion emphasises the properties of collisions in the regimes of low plasma temperature and low charge state of impurity ions. Particular attention is devoted to recycling of hydrogen atoms and molecules because of its powerful influence upon plasma properties adjacent to boundary surfaces.

January 1985

Table of Contents

1. INTRODUCTION

Radiative power losses arising from collisions of hot plasma electrons with impurity ions are important consequences of atomic collisions in fusion plasmas. So also are power losses and impurity release subsequent to charge exchange collisions between protons and hydrogen* atoms. However, until recently, emphasis has been placed upon the effects of atomic interactions within the hot core of a magnetically confined plasma and relatively little attention has been devoted to atomic and molecular collisions which occur in the region close to the boundary surface of the confinement vessel. The need to control impurity release in high power, long duration experiments coupled to the interest in divertors and pumped-limiters, for both experiments and reactor concepts, has stimulated studies of the boundary plasma and of the atomic processes which are important in this region.

The residence time for plasma particles within a confinement device must of course be finite so that the surface of the vessel is inevitably bombarded by plasma ions and electrons. Transport of plasma particles within the boundary is predominantly in the direction of the magnetic field so that the flux of escaping charged particles is strongly peaked at the divertor target or limiter plate. In the regime of present interest, incident ions are neutralised at the surface as a consequence of ion-surface interactions and (depending upon the ion energy together with the atomic species of both ion and surface) a substantial fraction of the incident ion flux can return as energetic backscattered atoms. In fusion relevant plasmas the predominant ion is a proton and the predominant backscattered particle a hydrogen atom. In steady state conditions there is conservation of particles so that those protons which do not contribute to backscattering are re-emitted as low energy detrapped neutrals which tend to be hydrogen molecules whose kinetic energy corresponds to the surface temperature. These neutral hydrogen particles traverse the plasma sheath which is collisionless and enter the boundary plasma which, in many envisaged and existing devices, is sufficiently dense and hot for ionisation to occur in the close proximity of the surface. This gives rise to a high degree of localised recycling of hydrogen plasma to the surface.

Localised recycling adjacent to the plasma collection surfaces enhances the fluxes of electrons and ions which are available to convect energy across the plasma sheath and to the surface. Depending upon the degree of plasma collisionality

---

* It is implicit, unless stated otherwise, that the discussion applies equally to all isotopes of hydrogen.

within the recycling region, this enhancement of particle fluxes ensures that a powerful flow of energy can reach the boundary surface without incurring the penalty of a high sheath temperature and sheath potential. The energy of ions incident upon the surface and the consequent yield of impurity atoms sputtered from the surface are thereby reduced. The boundary plasma drifts in the direction of the magnetic field and its maximum velocity (at the plasma sheath edge) is about equal to the ion sound speed. Localisation of sources of ionised hydrogen due to recycling in this downstream region results in a low flow velocity in the plasma upstream of the collection surface and a rapid acceleration of the flow within the recycling region. This spatial distribution of drift velocity impacts substantially upon the ability of the drifting boundary plasma to entrain ions and thereby to sweep them to the plasma collection surface. Impurity ion transport within the boundary is affected, the present understanding being that impurities which are ionised within the recycling region will be swept to the plasma collection surface but that this beneficial action is less likely in the upstream regions of the boundary plasma.

In addition to its effects upon plasma particle transport, hydrogen recycling provides a powerful local sink for plasma electron energy. Not only is electron energy dissipated by ionisation (although this energy is subsequently returned to the plasma collection surface in the form of the potential energy carried by the incident protons) but energy is also lost by excitation of neutral hydrogen. The plasma is transparent to most atomic radiation and hydrogen can radiate powerfully in the low temperature, high density, recycling region. Charge transfer between low temperature protons and hydrogen atoms affects the distribution of plasma ion energy and also the transport properties of the plasma ions both along and across the magnetic field. Indeed the influence of atomic and molecular processes is so substantial that in present high recycling divertor experiments (e.g. ASDEX) most of the energy entering the divertor is dissipated by atomic and molecular processes and only a small fraction is carried to the divertor target by charged particles.

The previous discussion has emphasised the role of localised recycling of hydrogen caused by plasma impact upon a boundary surface but similar atomic processes are relevant to issues associated with fuelling by gas puffing and, albeit with somewhat different emphasis, to fuelling by pellet injection.

Impurity atoms present in the boundary are also subjected to collisions with the charged particles of the plasma. In the case of helium the most significant effect is upon the gas exhaust capabilities of a reactor. Ionisation within the boundary plasma causes helium to recycle to the plasma collection surface in a

manner somewhat comparable to hydrogen so that the plasma acts as a powerful pump for gas. This pumping action opposes that of the vacuum pumps which must perforce be placed at the wall of the reactor in order to exhaust the helium.

Heavier impurity elements can be present in the plasma due to sputtering of the boundary surfaces and interest ranges from low atomic number elements such as beryllium and carbon through medium number elements such as silicon and iron to the high atomic number refractory metals such as tungsten. In addition, gaseous impurities such as oxygen are frequently encountered in experiments and it is conceivable that noble gases such as argon may be deliberately injected in order to cool the boundary plasma. The radiating ability of impurities increases markedly with increasing atomic number. It is also strongly related to the distribution of charge states amongst the impurity ions which is itself influenced by the residence time of these ions within the plasma. Both the energy with which impurity ions impact upon the plasma collection surface and the likelihood that they are entrained within the drifting boundary are sensitive to the charge state of the impurity. A knowledge of the charge state history of the impurity species is therefore crucial for the understanding of impurity control.

The interactive coupling between plasma properties and atomic processes has been comprehensively reviewed by Drawin[1] in the context of both a hot and cold plasma environment. In the more restricted region of the cool edge plasma detailed discussions of most of the mechanisms which link plasma conditions to atomic processes can be found in reviews by Harrison[2,3] but these earlier papers have been directed specifically towards the interests of the specialist in atomic collision physics. The objective of the present paper is to reverse the emphasis. It is hoped that the material selected will provide an informative background to those aspects of atomic collision physics which underly the cross section data and scaling relationships which are currently employed in plasma modelling. Both experimental and theoretical methods are outlined and the general characteristics of collision processes are illustrated by examples of measured data. Emphasis is placed upon interactions which are of significance in the plasma edge but the basic concepts apply throughout the whole of the plasma. The depth of discussion is perforce restricted but the reader is referred to review articles which provide ready access to detailed information.

2. ATOMIC COLLISIONS IN THE BOUNDARY PLASMA

The rate of atomic or molecular collisions with either a plasma electron or ion can be expressed as

$$\nu_A = n_A \, n\langle\sigma v\rangle \qquad (2.1)$$

where n_A and n are respectively the densities of the atomic species and of the plasma particles and $\langle\sigma v\rangle$ is the rate coefficient, i.e. the product of the reaction cross section $\sigma(v)$ and collision velocity v averaged over a distribution which can generally be assumed to be Maxwellian. Collisions with plasma electrons (e.g. ionisation, excitation and molecular dissociation) tend to be dominant because $v_e >> v_i$ but there are cases where ion-atom interactions have large cross sections at low collision velocity. Of particular significance are charge exchange collisions of the type $X + X^+ \rightleftarrows X^+ + X$ which are both symmetric (in atomic species) and resonant (in potential energy).

3. PROCESSES INVOLVING HYDROGEN ATOMS

The subject of collisions is conveniently introduced by reference to the hydrogen atom because this atom has only one bound electron.

3.1 Atomic Stucture of the Hydrogen Atom

It is desirable to refresh our appreciation of the simpler features of atomic structure in order to understand the significance of various processes and to understand the practical issues which impact upon the accuracy and availability of both the theoretical and experimental data base.

The energy of the single electron moving in an orbit around the positively charged nucleus is determined by four quantum numbers. The "principal" quantum number n describes the scale of the motion and the energy. The ground state of the atom is $n = 1$ and, at the ionisation threshold, $n \rightarrow \infty$. By analogy with classical mechanics, n determines the major axis of elliptic orbits around the Bohr atom. The "azimuthal" quantum number ℓ determines the angular momentum (i.e. $\ell(h/2\pi)$ atomic units) and ℓ has the values $(n - 1)\ (n - 2) \ldots 0$. Electrons with azimuthal quantum numbers equal to 0, 1, 2, 3, 4, etc. are referred to as s, p, and d etc. in compliance with the terminology "sharp", "principal" and "diffuse", etc. which derives from optical spectroscopy. The electron has a "magnetic" quantum number m_ℓ which describes its energy in a magnetic field and m_ℓ takes the values ℓ, $(\ell - 1)$, $(\ell - 2) \ldots -\ell$ so that the total number of energy states available to an electron with azimuthal quantum number ℓ is, in the presence of a magnetic field, equal to $(2\ell + 1)$.

Spontaneous transitions between levels are governed by selection rules which, whilst not absolutely rigid, nevertheless

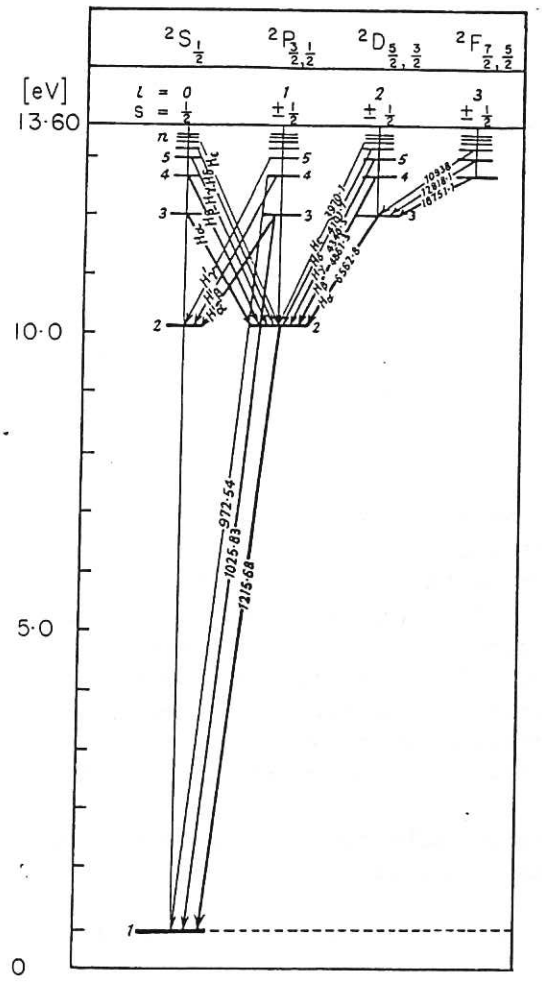

Fig. 1 The energy levels of the hydrogen atom in a field free environment.
The illustration is based upon Grotian[4]; transitions between sub-levels are not shown. Wavelengths are in Å. Note that the Lyman series corresponds to transitions from $n \geq 2$ to $n = 1$ and the Balmer series to $n \geq 3$ to $n = 2$. The Balmer series contains the H_α and H_β lines which arise respectively from $n = 3 \rightarrow 2$ and $n = 4 \rightarrow 2$ transitions.

determine the most prominent features of spontaneous radiative transitions within the atom. There is no restriction on the principal quantum number so that Δn can range from 0 to ∞. A transition is unlikely whenever the condition $\Delta \ell = \pm 1$ is violated. For example, transition between s to p and p to d levels are allowed whereas those between s to s and s to d are forbidden. These criteria give rise to the transitions of the hydrogen atom which (in a field free environment) are shown in Figure 1. Note that transitions from the level [$n = 2$; $\ell = 0$] to

the ground state are forbidden. This level (which is more generally designated 2s or $2^2S_{\frac{1}{2}}$) is metastable, its lifetime in a field free environment approaches 0.1 s.

The orbiting electron also spins around its own axis and a fourth quantum number $s = \pm \frac{1}{2}$ must be included to allow for the "mechanical momentum" of the spinning electron. The total mechanical moment of the atom arises therefore from a vectorial combination of the azimuthal and spin moments, namely

$$\vec{j} = \vec{\ell} + \vec{s}$$

where $\vec{\ell}$ is the momentum vector corresponding to $\ell(h/2\pi)$. Quantisation of the total moment is described by the "total" or "inner" quantum number j. Since the direction of electron spin can only be "co" or "counter" to the direction of its motion in orbit it is obvious that $\vec{s} = \pm \frac{1}{2}$ (units of momentum) so that $j = \ell \pm \frac{1}{2}$. With the exception of the s levels (for which $\ell = 0$) all of the levels of the hydrogen atom are split into two sub-levels (also called terms) which are separated by a small energy difference. This "multiplicity" is not shown in Figure 1.

The selection rule for j is $\Delta j = \pm 1$ or 0. The multiplicity of the level is given by

$(2s + 1)$ when $\ell > s$ or $(2\ell + 1)$ when $\ell < s$

so that the s levels of hydrogen are not split.

3.2 Electron Collisions with Hydrogen Atoms

Those plasma electrons whose energy exceeds the ionisation threshold of the atom (E_i) may impart sufficient energy to the bound electron for it to be removed completely from the influence of the Coulomb field of the proton. Ionisation from the ground state

$$e + H(1s) \rightarrow e + e + H^+ \qquad (1)$$

provides a substantial sink for kinetic energy of the plasma electrons because $E_i = 13.6$eV. Moreover the energy of the ejected electron is small (1 to 2 eV is typical for collisions pertinent to the boundary plasma) so that ejected electrons tend to dilute the energy content of the plasma. Recoil of the ion has a negligible effect upon the plasma.

The threshold energy E_{pq} for excitation from a lower atomic level p to upper level q is less than the ionisation threshold energy so that ionisation by plasma electrons is always accompanied by excitation. The excitation process

$$H(p) + e \rightarrow H(q) + e \qquad (2)$$

causes the plasma electron to lose an amount of kinetic energy (equal to the energy difference E_{pq} between the levels p and q) and it is obvious that only those plasma electrons whose energy is greater than E_{pq} can participate in such collisions. The excited state q has a finite lifetime associated with its spontaneous radiative decay,

$$H(q) \rightarrow H(p') + h\nu, \qquad (3)$$

to a lower level p' (for examples see Ref. 5). Here the photon energy $h\nu$ corresponds to the difference in the energy levels $q \rightarrow p'$ and, depending upon the decay characteristics, p' may or may not be the same level as p. The plasma is generally optically transparent to atomic radiation so that the energy associated with reaction (3) is lost to the walls of the vessel where it is absorbed. The spatial distribution of emitted photons is related to the direction of the colliding electron but the photon distribution within the bulk plasma can be assumed to be uniform in space. The collision scatters the plasma electron but the atom motion is unaffected.

The average time for collisions between plasma electrons and an atom in an excited level q is

$$\tau_q = (n\langle\sigma v_e\rangle_q)^{-1}. \qquad (3.1)$$

In plasmas where $n > 10^{14}/cm^3$, this collision time may be appreciably less than the lifetime for spontaneous radiative decay of all but the lower excited states of hydrogen. In such conditions super-elastic collisions

$$e + H(q) \rightarrow e + \Delta E + H(p') \qquad (4)$$

become important. The collision does not yield a photon but the potential energy stored in the excited atom H(q) is returned to the plasma electron. These de-exiting collisions reduce the population of excited hydrogen atoms.

Ionisation of excited H atoms is discussed in Section 7, the cross sections are large because the scaling is of the form $\sigma(v_e)_n \propto n^4$. Moreover the ionisation threshold energy decreases as $(E_i)_n \propto n^{-2}$ so that even electrons in the low energy tail of the plasma thermal distribution are able to ionise excited atoms. Ionisation of excited hydrogen

$$e + H(q) \rightarrow e + e + H^+ \qquad (5)$$

provides a second route by which the population of excited H atoms

is reduced. Collisional radiative (or multi-step) processes involving a balance between reactions (2), (3), (4) and (5) powerfully reduce radiative power losses from hydrogen atoms in a low temperature, high density edge plasma (see Refs. 2, 3, 6, 7 and 8). These effects are discussed in Section 10.1. The electron impact ionisation rate coefficient $S_i(g) = \langle \sigma_i v_e \rangle$ for ground state hydrogen and the coefficient S_{CR}, which includes enhancement of ionisation arising due to collisional radiative effects, are shown in Figure 2.

Protons can be destroyed by two-body radiative recombination with an electron

$$e + H^+ \rightarrow H(q) + h\nu. \qquad (6)$$

The photon carries away the excess energy of the interaction, i.e. the kinetic energy of the electron plus the energy of ionisation. The recombination rate coefficient for hydrogen $\alpha(T_e)$ is shown in Figure 3. It is very small except at low electron temperature ($k_B T_e$ < 1 eV) and high electron density so that the characteristic recombination time

$$\tau_\alpha = [n\,\alpha(T_e)]^{-1} \qquad (3.2)$$

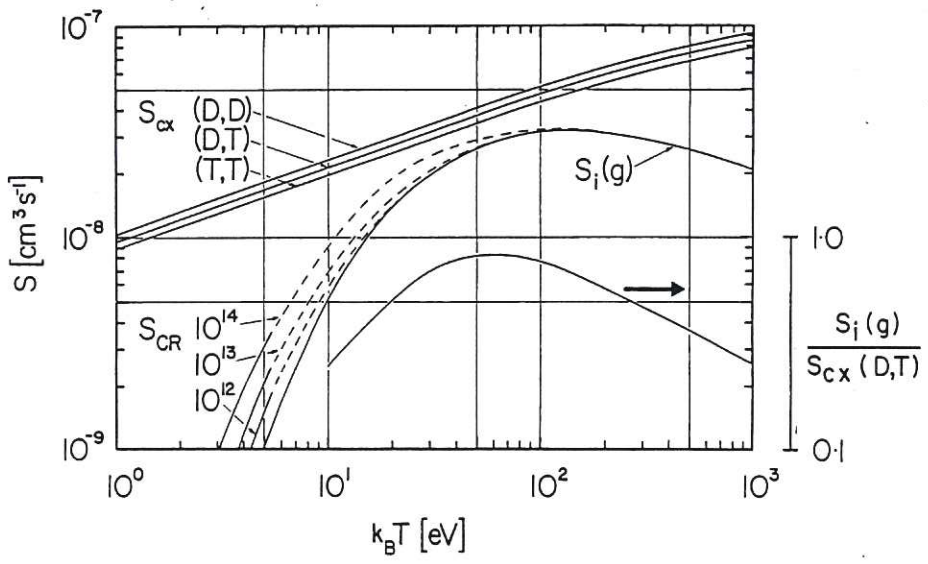

Fig. 2 Rate coefficients for electron ionisation and for proton charge exchange in collisions with hydrogen atoms. Data are taken from Harrison[3].
$S_i(g)$ refers to ionisation from the ground state of hydrogen whereas S_{CR} are collisional radiative ionisation coefficients for the electron density range 10^{12} to $10^{14}/cm^3$. The charge exchange rate coefficient is $S_{cx} = \langle \sigma_{cx} v_i \rangle$ and G is the ratio $S_i(g)/S_{cx}$.

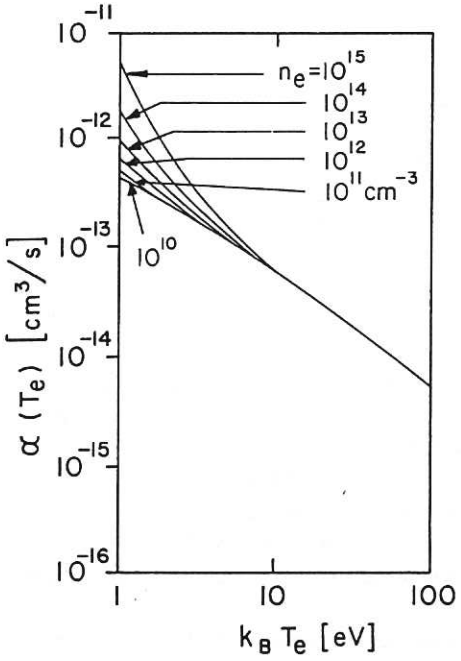

Fig.3 Collisional radiative recombination rate coefficient for $e + H^+$ collisions.
Data are taken from Janev et al[8].

is generally considerably longer than the time that the recycling proton resides within the plasma. Two-body radiative recombination of hydrogen is therefore not likely to be substantial within the boundary plasma.

Electron-proton recombination can in principle arise as a consequence of three-body collisions,

$$e + e + H^+ \rightarrow H(q) + e, \qquad (7)$$

but the electron density within the boundary plasma is insufficient for this process to be significant.

It is worthwhile noting that radiation due to free-free collisions

$$e + H^+ \rightarrow \text{bremsstrahlung radiation} \qquad (8)$$

is negligible in the boundary because of the relatively low electron temperature.

3.3 Charge Transfer between Hydrogen Atoms and Protons

Electron loss by a hydrogen atom and the equivalent process of electron capture by a plasma proton has unique significance because the rate coefficient for this species-symmetric and energy resonant reaction

$$H + H^+ \rightleftarrows H^+ + H \qquad (9)$$

is so large that it strongly influences the behaviour of the hydrogen recycling within the boundary plasma. By contrast, charge exchange between H^+ and H_2 molecules is neither symmetric nor resonant and such contributions are sufficiently small to be neglected. However electron impact dissociation of molecules (which is discussed in Section 5.2) does produce H atoms which can subsequently charge exchange with plasma protons.

During a charge exchange collision the parent hydrogen atom loses little kinetic energy but it becomes charged and the subsequent motion of the daughter proton is constrained by the magnetic field. The reverse applies to the parent plasma proton which becomes a daughter charge exchange atom whose energy is equal to that of the parent proton but whose trajectory tends to be randomly directed because it is no longer constrained by the magnetic field. When viewed in a specific direction, the depth of penetration into the plasma of many generations of daughter charge exchange atoms prior to their ionisation is reduced by the scattering action of charge exchange. In cases where there are many successive scattering events it is reasonable to determine the effective range, Δ_{cx}, on the basis of a diffusive transport of the daughter atoms. If the plasma is homogeneous it can be argued that

$$\Delta_{cx} = \left(\frac{S_{cx}}{3S_i}\right)^{\frac{1}{2}} \lambda_{cx}. \qquad (3.3)$$

Here $S_{cx} = \langle\sigma_{cx} v_i\rangle$ and $S_i = \langle\sigma_i v_e\rangle$ are respectively the rate coefficients for charge exchange and for electron impact ionisation and

$$\lambda_{cx} = \frac{\bar{v}_o}{n\, S_{cx}} \qquad (3.4)$$

is the mean free path for charge exchange of hydrogen atoms whose mean velocity is $\bar{v}_o$. The rate coefficients are shown in Figure 2 for a homogeneous Maxwellian plasma wherein $T_e = T_i$. The ratio $G = (S_i/S_{cx})$ is less than unity at all plasma temperatures and so it is evident that scattering of charge exchange daughter atoms appreciably attenuates the effective ionisation range of the neutral hydrogen.

4. ATOMIC PROCESSES INVOLVING HELIUM AND OTHER IMPURITY SPECIES

4.1 Structure of the Helium Atom and Ion

The helium atom has two electrons and in such simple atoms it is permissible to neglect coupling between the spin and momentum vectors associated with a particular electron and to account for the presence of two electrons by adding the azimuthal momentum and spin moment vectors independently. Thus $\vec{L} = (\vec{\ell}_1 + \vec{\ell}_2)$ and $\vec{S} = (\vec{s}_1 + \vec{s}_2)$. The total angular momentum is therefore $\vec{J} = \vec{L} + \vec{S}$. This is an example of LS (or Russel-Saunders) coupling* and the azimuthal quantum number L has the integral values $(\ell_1 - \ell_2)$, $(\ell_1 - \ell_2 + 1)$ .... $(\ell_1 + \ell_2)$. The spin quantum numbers are S = 0 or 1 because the electron spins may be aligned either anti-parallel or parallel.

The selection rules are

$\Delta L = 0, \pm 1$; $\Delta S = 0$, $\Delta J = 0 \pm 1$ (but $0 \rightarrow 0$ is forbidden)

and the multiplicity is

$(2S + 1)$ when $L \geq S$ or $(2L + 1)$ when $L < S$.

Levels corresponding to L = 0, 1, 2, 3, etc. are designated S, P, D, F, etc. and the conventional spectroscopic notation is

$$n^{(2S+1)}(L)_J \quad \text{e.g. } 1^1S_o,\ 3^3P_2, \text{ etc.}$$

This form of notation is also applied to the hydrogen atom although this atom has but one electron.

In the case of the helium atom there are two multiplicities namely 1 and 3. The energy levels, which are illustrated in Figure 4, clearly show the singlet and triplet branches. Both the 2^1S_0 and the 2^3S_1 levels are metastable but the metastability of the 2^3S_1 state is stronger because, not only does a transition to the ground state require that this electron violates the $\Delta\ell = \pm 1$ rule, but it also involves a change in multiplicity, i.e. a change in the spin direction of the bound electron.

The helium ion, He^+, is hydrogenic and its terms differ from the hydrogen atom only to the extent that the energy levels are scaled by a factor $Z^2 = 4$ where Z is the atomic number of

---

* For more complex coupling between jj the reader is referred to textbooks on atomic spectra and structure, for example Herzberg[9], Candler[10].

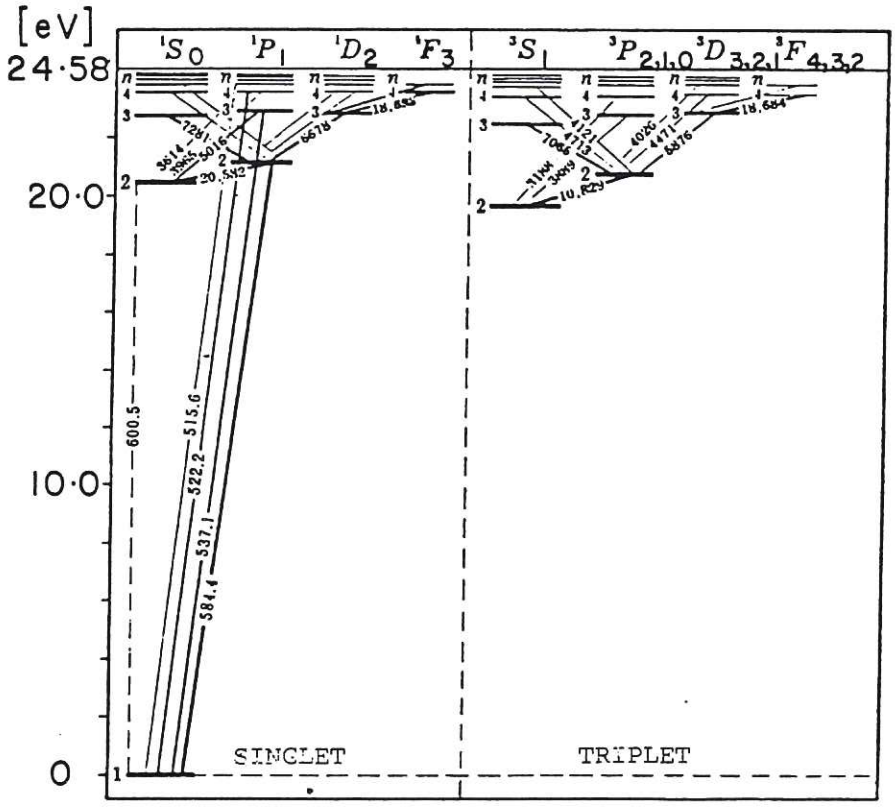

Fig. 4 The energy levels of the helium atom in a field free environment.
Illustration is based upon Grotian[4], transitions between sub-levels are not shown. Wavelengths are in Å.

helium. The same scaling rule can be applied to other hydrogenic ions, e.g. C^{5+}, O^{7+}, etc.

4.2 Structure of Complex Atomic Species

Differences in the structure of the simple species H (or He^+) and He are adequate to provide a framework for most of the following discussion. It is necessary only to note that the Pauli exclusion principle requires that no two electrons bound to the same atom may have identical quantum numbers. This ensures that two electrons with the same value of n and ℓ must have $s = +\frac{1}{2}$ and $s = -\frac{1}{2}$ and leads to the concept of electron shells which are related to the principle quantum number n, e.g.,

n	1	2	3
Shell designation	K	L	M
Number of electrons	2≡(2s)	8≡(2s+6p)	18≡(2s+6p+10d)

Note that the individual electrons are described in the same manner as in the hydrogen atom. Electrons in the K shell are most strongly bound and the binding energy decreases progressively as n increases.

4.3 Electron Collisions with Impurity Species

Collision processes similar to those in hydrogen atoms occur in the case of impurity elements but the situation is more complex because of the greater number of bound electrons. Electrons in the outermost shell of the atom (or ion) are less tightly bound than those in inner shells and so the outermost electrons participate most readily in excitation and ionisation. However, in many species, there are more inner electrons so that the net contribution from inner shells may well exceed that of the outer (for example see the total electron impact cross ionisation cross section for $Fe^{+} \rightarrow Fe^{2+}$ shown in Figure 16).

The presence of many bound electrons increases the number of possible collision processes. One such example is that the plasma electron may, in a single collision, eject more than one of the bound electrons of the impurity species X^{z+}, namely

$$e + X^{z+} \rightarrow e + ae + X^{(z + a)+} \qquad (10)$$

However, multiple ionisation is not likely to be particularly significant in the cool boundary plasma where ionisation by electron impact most probably proceeds in a stepwise manner i.e.

$$X^{o} \rightarrow X^{+} \rightarrow X^{2+} \dashrightarrow .$$

A more fundamentally significant process is the excitation of auto-ionising states

$$e + X^{z+} \rightarrow e + X^{z+*} \rightarrow e + e + X^{(z + 1)+} \qquad (11)$$

This occurs when an inner bound electron is excited to a level whose bound energy, $E_{*}(in)$, exceeds the ionisation threshold of the outer electron, $E_{i}(out)$. When the inner electron level decays, the energy associated with its photon can be coupled to an outer bound electron which is then ejected with an energy $[E_{*}(in) - E_{i}(out)]$. The contribution of autoionisation to the total electron impact cross section for ionisation can be seen in Figure 20.

The reverse of autoionisation is dielectronic recombination

$$e + X^{z+} \rightarrow e + X^{z+*} \equiv \left(X^{(z - 1)+**}\right) \rightarrow X^{(z - 1)+*} + h\nu \; . \qquad (12)$$

In this type of collision a plasma electron loses energy by exciting the ion X^{z+} but, after the collision, the incident electron has insufficient energy to escape from the Coulomb field of the ion. Thus, for a short time, there exists a doubly excited species $\left(X^{(z-1)+**}\right)$. If the system can become stable by emitting a photon without suffering auto-ionisation then the electron and ion will have recombined. The effect is really a by-product of excitation and its contributions are significant when the electron energies lie close to the excitation threshold. The rate coefficient, illustrated here in Figure 5 for the case of $Ne^{6+} \rightarrow Ne^{5+}$, follows somewhat the shape of an excitation coefficient and it peaks at a relatively high electron temperature. It thus differs significantly from the radiative recombination coefficient which decreases monotonically with increasing temperature. Even so, dielectronic recombination within the boundary is unlikely to have a substantial effect upon plasma conditions because of the relatively short residence time of the impurity ions.

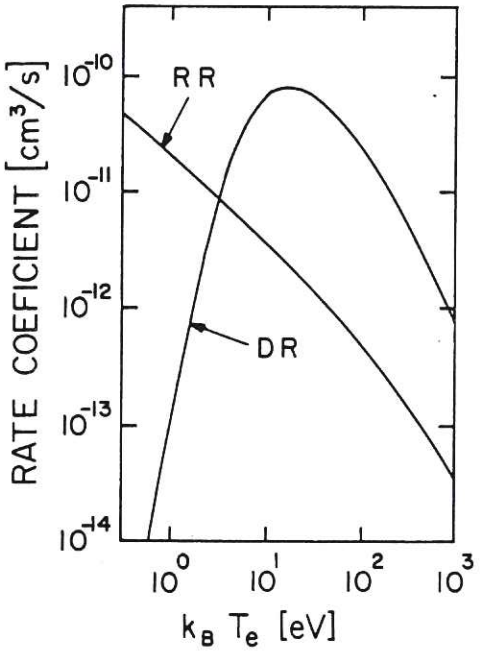

Fig. 5 Comparison of the rate coefficient for collisional dielectronic recombination compared with that for collisional radiative recombination.
Data are for $Ne^{6+} \rightarrow Ne^{5+}$ and are taken from Jacobs et al[11].
Curve RR shows the collisional radiative coefficient but only the most dominant contribution to dielectronic recombination is shown by curve DR, i.e. those due to transitions $n'\ell' \rightarrow n\ell$ where $n' = n = 2$, $\ell' = 2p$ and $\ell = 2s$.

4.4 Collisions between Hydrogen and Impurity Ions

Collisions between impurity ions and their associated atoms can generally be neglected. For example the rate coefficient for the symmetrical, resonant charge exchange reaction in helium,

$$He + He^{+} \rightleftarrows He^{+} + He \qquad (13)$$

is large even at low collision velocity but the effect upon He atom transport is slight because of the relatively small concentration of He^{+} in the boundary plasma.

Collisions between H atoms and impurity ions cannot be symmetric but in some cases they tend to be energy resonant. A typical example, discussed in Section 9, is

$$C^{6+} + H \rightarrow C^{5+}(n = 4) + H^{+} \qquad (14)$$

for which the cross section data are shown in Figure 28. At relevant H atom collision energies ($\sim$ 100 eV) the rate coefficient is $\sim 10^{-8}$ cm^3/s which exceeds by many orders that for two body radiative recombination (i.e. $e + C^{6+}$) which at $k_B T_e$ = 100 eV is about 10^{-11} cm^3/s. This type of collision is often called "charge exchange recombination" but its formal name is "electron capture into excited states". The excited C ion subsequently emits a photon when it decays. The influence of collisions of this type upon the charge state population of impurity ions is considered in Section 10.2.

Cross sections for the reverse type of reaction, e.g.

$$C^{5+} + H^{+} \rightarrow C^{6+} + H \qquad (15)$$

tend to be small in the proton energy regime of interest because Coulomb repulsion between the colliding ions reduces the interaction probability at low energy. In addition, the tendency to energy resonance can (as in the case of reaction 15) be dominated by a specific excited state of the impurity ion and such excited ions constitute but a small fraction of the impurity population.

Other processes such as proton impact ionisation,

$$H^{+} + X^{z+} \rightarrow H^{+} + X^{(z+1)+} + e \qquad (16)$$

or hydrogen atom stripping

$$H + X^{z+} \rightarrow H^{+} + X^{z+} + e \qquad (17)$$

can be neglected in the low ion temperature region of the boundary. It should however be stressed that such neglect is not

valid if there are significant numbers of energetic particles present in the boundary region, for example, atoms and ions from injected beams, energetic particles in banana orbits (particularly α-particles). Indeed reactions of the type (14), (16) and (17) have been invoked in numerous diagnostic studies based upon injected beams of atoms or ions.

5. PROCESSES INVOLVING HYDROGEN MOLECULES

5.1 The Structure of the Hydrogen Molecule

At infinite separation the components of the H_2 molecule have the properties of individual atoms. However at close internuclear distances there is a complex interplay of forces between the two nuclei, between the two electrons and between each electron and the nucleus of the other atom. The two charged nuclei exert a repulsive force which is always dominant at close internuclear separation but electrons in certain configurations can exert an opposing attractive force so that a stable molecule can be formed. Energy transferred during electron impact can change the symmetry of the electron configuration so that the repulsive force is no longer opposed and the molecule dissociates into two atoms. Dissociation is sometimes accompanied by emission of a photon. A stable configuration is also possible when only one electron and two protons are bound so that a stable H_2^+ molecule can be formed by electron impact upon H_2.

The electronic levels of the hydrogen molecule are too complex to discuss in detail. Suffice to say here that the designations Σ, Π, Δ correspond to S, P, D terms in helium but that they are determined by momentum quantum numbers which refer to the direction of the molecular axis. The multiplicity relates to the parallel or anti-parallel directions of the electron spin in the two atoms which make up the molecule. The subscripts u (ungerade = uneven) and g (gerade = even) refer to the symmetry effects which influence transition probabilities. In homonuclear molecules (such as H_2) the transitions $g \rightarrow u$, $u \rightarrow g$ are allowed but neither $g \rightarrow g$ nor $u \rightarrow u$ are allowed. The reader is referred to Gaydon[12] for a concise introduction to the subject.

A diagram of the potential energy curves (i.e. the interaction energy as a function of inter-nuclear separtion) is shown in Figure 6. The molecule rotates about its axis but in the present context the effect can be neglected. The nuclei also vibrate in the direction of the molecular axis and this effect is important. Vibration is quantised and the range of inter-nuclear separation associated with the lowest vibrational state of H_2 is indicated in Figure 5 by the vertical lines A and B. The time for an electronic transition ($\sim 10^{-16}$s) is much smaller than that of

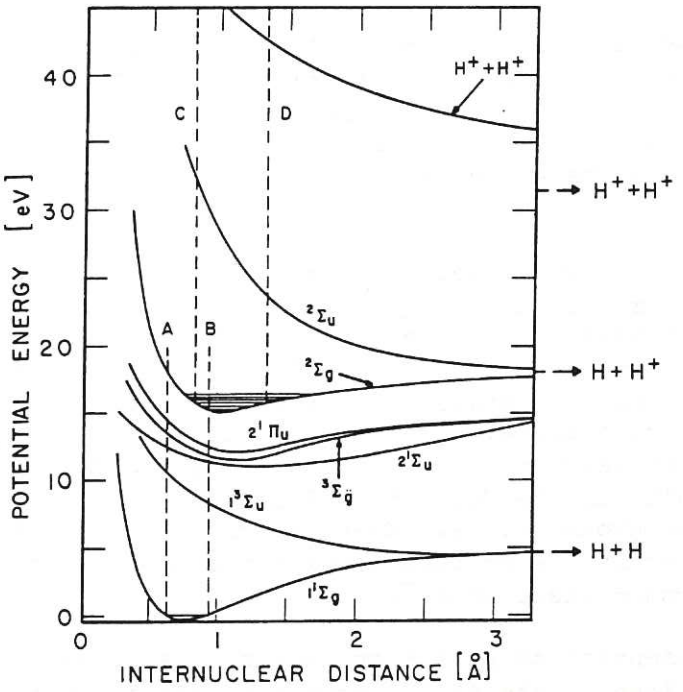

Fig. 6 Potential energy of H_2 and H_2^+ molecules as a function of internuclear separation.
The Frank-Condon region of H_2 is shown by the vertical lines A and B and that for H_2^+ by C and D.
Data on energy levels are taken from Oak Ridge National Laboratory Report ORNL 3113 (Ref. 13).
The arrows on the righthand side show the potential energy at infinite internuclear separation.

a period of nuclear vibration ($\sim 10^{-14}$ s) so that there is negligible motion of the nuclei during an electronic transition. An incident electron is most likely to encounter the nuclei at the turning points in their motion which coincide with A or B. A valuable criterion introduced independently by Frank and Condon is that transitions between electronic levels are most likely to occur where the vertical lines A or B intersect the potential energy curves which identify the levels.

To describe the effects of electron collisions with molecular hydrogen let us consider the scenario in which the energy of the incident electron is progressively increased. The first transition from the $1^1\Sigma_g$ ground state of H_2 occurs at about 8.5 eV where the vertical B line intersects the $1^3\Sigma_u$ state of H_2. This state is repulsive and dissociates into two ground state H atoms. At the Frank-Condon edge (B) the potential energy of the $1^3\Sigma_u$ state is about 4 eV higher than that of the $1^1\Sigma_g$ curve when this is at

infinite internuclear separation. Thus the transition, which extracts about 8.5 eV from the kinetic energy of the plasma electrons, causes a decrease of about 4 eV in the potential energy of the H + H system which reappears in the form of kinetic energy which is equally shared between the H_2 molecule dissociation products.

When the incident electron energy is increased to 11.75 eV the B line intersects the $2\,^1\Sigma_u$ curve. The molecule can then radiate by a transition to the ground state (i.e. $u \rightarrow g$ is allowed and there is no change in multiplicity). At a slightly higher energy the $2\,^3\Sigma_g$ state is excited and this can radiate to the $1\,^3\Sigma_u$ repulsive state. Thus this latter transition produces a photon and also results in dissociation. Proceeding to higher energies results in the formation of the $2\,^1\Pi_u$ state which can radiate to the ground state. Eventually, at higher electron energy, an electron is ejected leaving the molecule in the stable $^2\Sigma_g$ ground state of H_2^+.

It is essential to note that internuclear separation of the ground vibrational state of H_2^+ does not coincide with that of H_2 and according to the Frank-Condon criteria, whenever an H_2^+ ion is formed by electron impact upon vibrationally unexcited neutral H_2, the ion is inevitably vibrationally excited. The peak of the vibrational distribution is expected to coincide with the state $v \approx 2$ so that a second Frank-Condon region, denoted in Figure 6 by the vertical lines C and D, must be used to describe electronic transitions in H_2^+.

Electron impact upon an H_2^+ ion can excite the lowest lying repulsive $^2\Sigma_u$ state. The intersection point of this curve and the Frank-Condon edge D indicates that the $^2\Sigma_u$ state dissociates into an H(1s) atom and a proton, each particle having about 4.5 eV energy. The incident electron energy required to dissociate H_2^+ is extremely sensitive to the distribution of the vibrational states of H_2^+, a small population of the higher states dominates the transition probability. Transitions to higher electronic levels of H_2^+ occur at higher incident electron energy, some transitions give rise to radiation but all higher states are, in effect, repulsive and yield an excited H* atom and a proton. At the highest relevant energy (~ 28 eV) the molecule breaks up into two protons each having about 6 eV energy.

The preceding scenario is somewhat simplistic. Transitions at the inner edge of the Frank-Condon region (lines A and C) have not been considered. Moreover, a significant issue in the context of the boundary plasma is the lack of knowledge regarding the population of the vibrational states of neutral H_2 molecules involved in recycling.

5.2 Electron Collisions with Hydrogen Molecules

Collisions between plasma electrons and neutral H_2 can, in progressive order of their threshold energies, give rise to the following interactions;

$$e + H_2 \rightarrow H + H^- \qquad \text{[dissociative attachment]} \qquad (18)$$

$$e + H_2 \rightarrow e + H + H \qquad \text{[dissociation]} \qquad (19)$$

$$e + H_2 \rightarrow e + H_2^* \rightarrow e + H_2 + h\nu \qquad \text{[excitation]} \qquad (20)$$

$$e + H_2 \rightarrow e + H_2^* \rightarrow e + H + H + h\nu \qquad \text{[dissociative excitation]} \qquad (21)$$

$$e + H_2 \rightarrow H_2^+ + e + e \qquad \text{[ionisation]} \qquad (22)$$

$$e + H_2 \rightarrow H^+ + H + e + e \qquad \text{[dissociative ionisation]} \qquad (23)$$

$$e + H_2 \rightarrow H^+ + H^+ + 2e + e \qquad \text{[dissociative ionisation]} \qquad (24)$$

Excitation of the electronic levels of the molecule together with ionisation of the molecule act as energy sinks for the plasma electrons but in addition the plasma electrons dissipate energy in collisions which result in dissociation. In the context of plasma transport the molecule can be regarded as a potential source of H atom (or proton) momentum. For example when the H_2 molecule is dissociated into H + H by electron impact then two atoms each with an energy of 2.2 eV are released for the expenditure of 8.8 eV electron energy. The dissociation products can be assumed to have a random spatial distribution within the plasma.

Rate coefficients of these reactions are shown in Figure 7 and the most significant are (a) dissociation S_d^o [this coefficient includes contributions from reactions (19) and (21)], (b) ionisation S_{io} [arising from reaction (22)] and (c) dissociative ionisation S_{di} [arising from reaction (23)].

In the case of H_2^+ the possible reactions, again in progressive ranking of threshold energy, are

$$e + H_2^+ \rightarrow H + H \qquad \text{[dissociative recombination]} \qquad (25)$$

$$e + H_2^+ \rightarrow e + H^+ + H \qquad \text{[dissociation]} \qquad (26)$$

$$e + H_2^+ \rightarrow e + H_2^{+*} \rightarrow e + H^+ + H + h\nu \qquad \text{[dissociative excitation]} \qquad (27)$$

$$e + H_2^+ \rightarrow e + e + H^+ + H^+ \qquad \text{[dissociative ionisation]} \qquad (28)$$

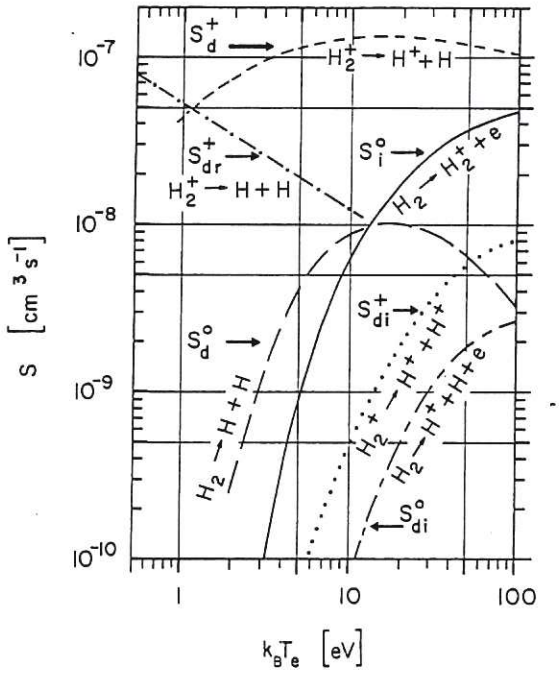

Fig. 7 Dominant rate coefficients for electron collisions with H_2 and H_2^+ plotted as a function of electron temperature. Symbols are defined in the text and data are taken from Harrison[3].

The rate coefficient for dissociation S_d^+ [reaction (26) and (27)] is dominant whereas the rate coefficients for dissociative recombination S_{dr}^+ [reaction (25)] can be neglected except at very low temperature. Dissociative ionisation S_{di}^+ [reaction (28)] has only a minor influence upon the characteristics of the boundary plasma.

It is sometimes convenient to express the rate coefficient $S^o(H^+)$ for the total formation of protons due to collision of electrons with H_2 in the form

$$S^o(H^+) \approx S_i^o\left(\frac{S_d^+ + 2S_{di}^+}{S_d^+ + S_{di}^+}\right) + S_{di}^o \qquad (5.1)$$

and the coefficient for the formation of H atoms, $S^o(H)$ in the form

$$S^o(H) \approx 2S_d^o + S_{di}^o + S_i^o\left(\frac{S_d^+}{S_d^+ + S_{di}^+}\right). \qquad (5.2)$$

Collisions between H_2^+ and H_2 give rise to the molecule H_3^+,

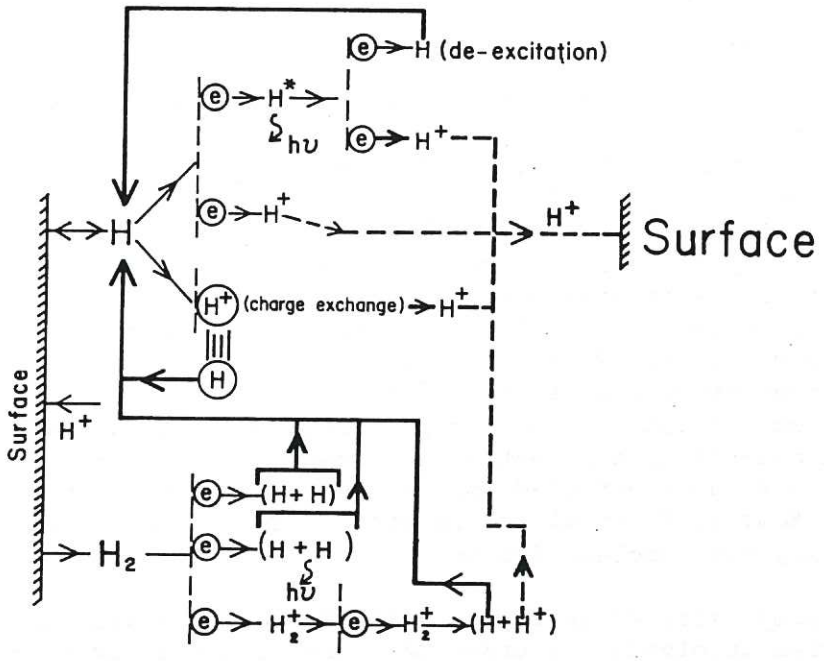

Fig. 8 Schematic representation of the dominant atomic and molecular collision processes associated with the recycling of hydrogen.

$$H_2^+ + H_2 \rightarrow H_3^+ + H, \qquad (29)$$

but the rate coefficient is about 10^{-2} less than that for the destruction of H_2^+ by electron impact and so the reaction will be significant only when the density of neutral H_2 is much higher than that of the plasma electrons.

The atomic and molecular processes which are dominant in hydrogen recycling are indicated schematically in Figure 8.

6. INTRODUCTION TO ATOMIC COLLISION PHYSICS

Some background knowledge of the physics processes which influences the magnitude and energy dependence of atomic collision probabilities helps the plasma modeller to identify the most significant interactions which pertain in a particular plasma environment. This paper aims to fulfil this requirement by providing a highly simplified outline of the nature of the more common atomic interactions and of some generalised formulae which are frequently used to predict cross section data. No attempt is made to provide a comprehensive data base but trends which are inherent to specific types of collision processes are illustrated

by examples of data for species which have particular relevance to the boundary plasma.

It must be stressed that this approach neglects many fundamental details of atomic collision physics but the field of is very well documented elsewhere. The most comprehensive discourse on theory and experiment is provided in 5 volumes by Massey, Burhop and Gilbody[14]. The present author has found McDaniel[15] to be particularly helpful but the choice of literature is wide and personal taste is in some measure invidious. There are several collections of review articles which relate specifically to the atomic and molecular needs of fusion. The proceedings of earlier NATO Advanced Study Institutes[16,17,18] are valuable examples. The multifarious influence of atomic processes on both natural and man made environments have recently been comprehensively reviewed in a series of 5 volumes entitled Applied Atomic Collision Physics edited by Massey, McDaniel and Bederson[19] and volume 2 deals specifically with nuclear fusion.

The complexity of an atomic collision depends upon the type of particles involved. In order of increasing complexity these are firstly photon and secondly electron collisions with either atoms or ions. Then follows collisions with molecules and finally collisions involving two particles each of which has atomic structure (one such example being charge exchange between H atoms and partially stripped impurity ions). The energy at which particles collide is also important; in general the interactions are complicated in the relatively low energy regime which is pertinent to the boundary plasma. For simplicity the subject is introduced by a discussion of inelastic collisions of electrons with atoms or ions but the principles are also applicable to electron-molecule and to ion-atom or ion-ion collisions. The influence of the plasma environment upon the basic collision processes and the methods employed to estimate collision rates are discussed briefly in Section 10.

6.1 Theory of Inelastic Electron Collisions

The inelastic process of excitation or ionisation requires that the incident electron transfers sufficient of its kinetic energy to a bound electron for the latter to be raised to a higher excited state or else to be ejected from the influence of the Coulomb field of the charged nucleus. The first theoretical treatment of ionisation (Thomson[20]) is based upon a classical model in which a stationary electron is approached from infinity by a moving electron with energy E. At a particular impact parameter (indicated by r in Figure 9) the amount of energy exchanged due to a single Coulomb collision is

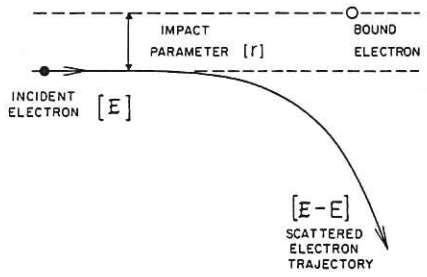

Fig. 9 Trajectory of an inelastically scattered electron. The impact parameter is r and the threshold energy of the atomic transition is E.

$$\Delta E = \frac{E}{1 + (rE/e^2)^2} \qquad (6.1)$$

where e is the electronic charge. Thomson assumed that the probability of ionisation is unity when ΔE is equal to or greater than the theshold energy for ionisation E_i. The classical electron impact cross section can then be expressed as

$$\sigma_{cl} = 4\xi \left(\frac{E_{i,H}}{E_i}\right)^2 \left(\frac{E_i}{E}\right) \left(1 - \frac{E_i}{E}\right) \pi a_o^2, \qquad (6.2)$$

where $E_{i,H}$ is the ionisation energy of the H atom, $a_o = 0.53 \times 10^{-8}$ cm is the radius of the Bohr atom and ξ is the effective number of bound electrons which can contribute to the interaction. The characteristics of this cross section are that its magnitude increases linearly with excess incident energy$(E - E_i)$ in the regime close to theshold. The energy dependence becomes progressively weaker at higher energies so that the cross section peaks at $E = 2E_i$ and when $E >> E_i$ the cross section decreases as (E_i/E).

The preceding aproach is clearly over simplistic. In classical terms the collision should be treated as a many body problem (three body even in the simplest case of a hydrogen atom) but, more significantly, the scale of the collision system requires that the problem be treated by quantum theory. Nevertheless the simple classical cross section given in Eq. (6.2) has formed the basis of many semi-empirical expressions used in plasma modelling. For example it shows clearly the scaling relationship

$$\sigma_{scaled} = \sigma \left(\frac{E_i}{E_{i,H}}\right)^2 \xi^{-1} = \text{function } (E/E_i) \qquad (6.3)$$

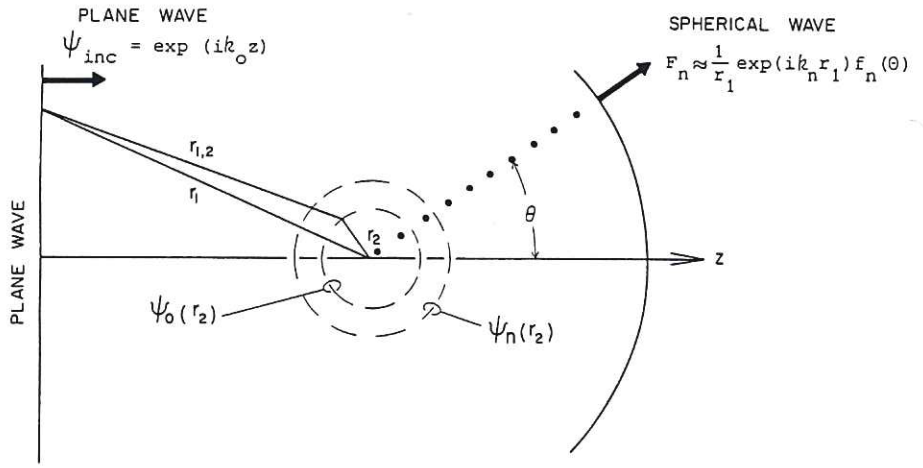

Fig. 10 Illustration of inelastic scattering of electrons based upon the quantum theory treatment.

Such scaling, which is supported by quantum theory, is used extensively for comparing experimental data and for extrapolation to species for which no measurement is available.

The quantum theory concept of inelastic electron-atom (or electron-ion) collisions is illustrated schematically in Figure 10. The method can be briefly outlined as follows. Consider that the atom (or ion) resides in an infinitely extending, uniform intensity beam of mono-energetic electrons. The incoming electrons which move in the z direction have an energy E when they are at large distances from the atom and here they are represented by a plane wave whose wave number is

$$k_o = 2\pi/\lambda_o = 2\pi\, m_e\, v_o/h = (2\pi/h)\,\sqrt{2m_e E} \qquad (6.4)$$

where m_e is the electron mass, v_o the initial velocity and h is Planck's constant. The wave function of these electrons is $\psi_{inc}(z) = \exp(ik_o z)$. The time independent wave equation of the collision system which includes both the incident electron and the atom (which for simplicity is taken to be an H atom) is

$$\left[-\frac{h^2}{8\pi^2 m_e}\left(\nabla_1^2 + \nabla_2^2\right) + \left(E_{SYS} - V(r_1,r_2)\right)\right] \Psi(r_1,r_2) = 0 \qquad (6.5)$$

Here the suffixes 1 and 2 refer respectively to the incident and to the atomic electron, the energy of the system is

$$E_{SYS} = E + E_{a,o} \qquad (6.6)$$

where $E_{a,o}$ is the potential energy of the atom in its initial

state. The interaction potential energy operator is

$$V(r_1,r_2) = -\frac{e^2}{r_1} - \frac{e^2}{r_2} + \frac{e^2}{r_{1,2}} \qquad (6.7)$$

where r_1 and r_2 are respectively the co-ordinates of the incident and atomic electron and $r_{1,2}$ is the distance between electrons. The function $\Psi(r_1,r_2)$ may be expanded over the excited and continuum states of the atom in the form

$$\Psi(r_1,r_2) = \left(\sum_n + \int\right) \phi_n(r_2)\ F_n(r_1) \qquad (6.8)$$

where the summation pertains to the bound states and the integration to the continuum states of the atomic electron. The functions of $\phi_n(r_2)$ are the wave functions of the hydrogen atom in state n. It can be shown that at large values of r_1 the function $F_n(r_1)$ is described by a wave number

$$k_n = (2\pi/h)\sqrt{2m_e(E_o-E_n)} \qquad (6.9)$$

This wave function therefore corresponds to free electrons which have lost an amount of kinetic energy corresponding to a change in the internal energy of the atom equal to a transition from the initial o state to the final n state. Clearly this represents the inelastically scattered incident electrons. At large values of r_1 the wave function which represents electrons that have been inelastically scattered through an angle θ must have the form of an outgoing spherical wave,

$$F_n \sim r_1^{-1} \exp(ik_n r_1)\ f_n(\theta) \qquad (6.10)$$

whereas the elastically scattered electrons are represented by

$$F_n \sim \exp(ik_o z) + r_1^{-1} \exp(ik_o r_1) f_o(\theta). \qquad (6.11)$$

The number of inelastically scattered electrons which cross a unit area of the surface of a sphere (of radius large r_1) in unit time is proportional to $k_n r_1^{-2} |f_n|^2$ whereas the associated flux density of electrons incident upon the atom is proportional to k_o. The differential cross section $I_{on}(\theta)d\Omega$ for those transitions $o \to n$ which cause scattering into a solid angle $d\Omega$ can be defined as the ratio of these flux densities so that

$$I_{on}(\theta)\ d\Omega = \frac{k_n}{k_o} \left| f_n(\theta)\right|^2 d\Omega \qquad (6.12)$$

Integration over the angles θ and ϕ of the spherical polar co-ordinate system yields the total cross section

$$\sigma_{on} = \int_o^{2\pi} \int_o^{\pi} I_{on}(\theta) \sin\theta\ d\theta\ d\phi \qquad (6.13)$$

Solution of the problem therefore requires that the asymptotic form (i.e. $r_1 \to \infty$) of the function $f_n(\theta)$ be determined but this is not amenable to precise calculation because this would involve an infinite number of coupled differential equations associated with the atomic states n. Success in this field has therefore been in large measure due to the informed approximations that have been invoked. The most frequently used approach is the Born approximation[21]. The basic simplifications made by Born are that (a) the incident electrons can be represented by a plane wave which is not distored by the influence of the unscreened charge of nucleus, (b) transition from an initial state (o) to a final (n) state of the atom is direct so that the effects of intermediate states are not significant and finally (c) the outgoing wave of inelastically scattered electrons is not distorted by interactions with the atom (or ion) in its final state. In effect the neglect of wave distortion implies that Born's approximation relates specifically to high energy collisions. Nevertheless the Born approximation and its many variants have been remarkably successful even at modest collision energies. The approach is used here to illustrate the high energy dependence of cross sections for excitation and ionisation.

It is convenient to transform from angular to momentum variables such that the change in momentum $(h/2\pi)\,K$ of the incident electron which is scattered through an angle θ can be expressed in terms of

$$K = (k_o^{\,2} + k_n^{\,2} - 2k_o\,k_n\cos\theta)^{1/2}. \qquad (6.14)$$

The limits of K correspond to

$$K_{max} = k_o + k_n(\Theta=\pi) \text{ and } K_{min} = k_o - k_n(\theta=\pi).$$

However Bethe[22] argued that an upper limit

$$K_o = (2\pi/h)\sqrt{m_e E_{i,o}}$$

can be imposed because at high incident energy the electrons lose only a small fraction of their momentum and are scattered through only a small angle; here $E_{i,o}$ is the ionisation threshold energy of the atom in its initial state. The total cross section for excitation of the o to n state by high energy electrons can be expressed (see Refs. 14 and 15) as

$$\sigma_{on} \simeq \frac{128\pi^5 m_e^{\,2} e^4}{k_o^{\,2} h^4} \int_{K_{min}}^{K_o} \left[K^{-1}|\chi_{on}|^2 + \frac{K}{4}|(\chi^2)_{on}|^2 + \ldots\right] dK \qquad (6.15)$$

where the matrix elements χ_{on}, χ^2_{on} are given by

$$(\chi^s)_{on} = \int \chi^s \psi_n^* \psi_o \, dr_2 . \qquad (6.16)$$

Here $\psi_o(r_2)$ is the wave function of the atom in its initial state and $\psi_n^*(r_2)$ is the complex conjugate of the wave function of the final state n. For optically allowed transitions ($\Delta\ell = 1$) the first (electric dipole) term of Eq. (6.15) does not vanish and so the remaining terms in the expansion can be neglected. Thus

$$\sigma_{on}^{dipole} \simeq \frac{16\pi^3 e^4}{h^2 v_o^2} |\chi_{on}|^2 \log \left(\frac{2m_e v_o^2}{E_{on}} \right) \qquad (6.17)$$

where χ_{on} is the energy difference between levels o and n. Note that $\sigma_{on}^{dipole} \propto v_o^{-2} \log v_o^2$ [i.e. $E^{-1} \log E$].

In the case of optically forbidden transitions ($\Delta\ell = 0$ or 2) then the dipole moment in Eq. (6.15) vanishes and the quadrupole moment becomes dominant so that

$$\sigma_{on}^{quad} \simeq \frac{32\pi^5 m_e e^4}{h^4 v_o^2} |(\chi^2)_{on}|^2 E_{i,o} \qquad (6.18)$$

and the high energy dependence is proportional to v_o^{-2}, [i.e. E^{-1}].

The high energy behaviour of the cross section for ionisation is comparable with that for the excitation of allowed transitions

$$\sigma_i \simeq \frac{2\pi e^4}{m_e v_o^2} \frac{c}{E_{i,o}} \log \left(\frac{2m_e v_o^2}{C} \right) . \qquad (6.19)$$

If k_i is the wave number of the ejected electron then

$$c = \int |\chi_{o,k_i}|^2 \, d\, k_i \qquad (6.20)$$

and the energy C is about one tenth of $E_{i,o}$.

Much effort has been expended in extending the quantum theory approach to lower energies. It is clear from classical arguments that inelastic collisions in the low energy regime (i.e. where E is only slightly greater than E_n) occur via closely coupled interactions between the incident and the bound electron. Moreover the trajectory of the incident electron (and also of the slow atomic electron ejected in ionisation) will be significantly influenced by both electron-electron interactions and by the unscreened field of the nucleus. These problems have been studied in detail. The incident electron has been allowed to see the partially screened

Coulomb field of the nucleus (Coulomb-Born), polarization of the atomic charge distribution by the presence of the incident electron has been considered, the influence of the many interacting states of the atom (or ion) has been assessed (Close Coupling), the incident electron has been allowed to change places with the bound electron (Exchange), the final (n) states have been coupled to the scattered electron and the transitory trapping of the incident electron within the partially screened field of the nucleus has been investigated (Dielectronic effects). Recent general surveys of theoretical treatments of electron collisions can be found in Joachain[23].

For present purposes it is sufficient to note that treatments based upon quantum theory demonstrate, in the specific cases of ionisation and of excitation of allowed transitions, that the classical approach over-estimates the coupling of energy when the impact parameter of the incident electron is small but it underestimates the energy coupling at larger impact parameters. As a consequence the peak value of the classical Thomson cross section is too large and too close to the threshold and, in the high energy regime ($\mathcal{E} > E$), the classical energy dependence $[\sigma_{cl} \propto \mathcal{E}^{-1}]$ is too strong. The high energy behaviour is more accurately described by the Born approximation as $\sigma_B \propto \mathcal{E}^{-1} \log \mathcal{E}$. Excitation of a forbidden transition which does not also involve a change in multiplicity is predicted to have a different high energy dependence, namely $\sigma_{on} \propto \mathcal{E}^{-1}$ and in this respect it is comparable to the classical behaviour. If a disallowed transition also involves a change in multiplicity, then the dependence $\sigma_{on} \propto \mathcal{E}^{-3}$ is expected at high energy and the cross section is very strongly peaked in the regime close to the threshold. The marked difference at low collision energy is to be expected because a change in multiplicity involves a change in the spin of the bound electron and this is likely to occur in closely coupled interactions between the bound and incident electron.

6.2 Semi-empirical Cross Sections used in Plasma Modelling

Despite the substantial number of detailed calculations of excitation and ionisation cross sections the plasma modeller is often forced to employ less precise methods. Data for large numbers of atomic processes are required and furthermore data in the low energy regime are of greatest significance (see the discussion of rate coefficients in Section 10). In addition to the complexities encountered at low collision energy, quantum theory calculations become significantly less certain as the number of bound electrons increases. The modeller thererefore tends to use semi-empirical data which are based upon the general energy dependences identified by theory but which are quantified by comparison with experiment. A number of semi-empirical methods have been evolved and these have been reviewed by Kato[24] and by Itikawa and

Kato[25]. Most ionisation data are derived from modifications of the classical cross section σ_{cl} such that (a) the semi-empirical cross sections display an $[E^{-1} \ln (E)]$ dependence at high energy and (b) that the position and magnitude of their peaks comply more closely with the trends identified in measured data. The semi-empirical formulation of Lotz[26] is probably the most widely applied and it takes the form

$$\sigma_i = \sum_{j=1}^{J} a_j \xi_j \frac{\ln(E/E_j)}{E E_j} \left\{1-b_j \exp\left[-c_j(E/E_j-1)\right]\right\} \qquad (6.21)$$

Here E_j is the binding energy of a "j"electron in the j-th sub-shell (j has the values $1 \rightarrow J$ where $j = 1$ corresponds to the outermost sub-shell), ξ_j is the number of equivalent electrons in the j-sub-shell and a_j, b_j, c_j are fitting parameters derived by comparison with the limited experimental data base available to Lotz. This approach has served well in the cases where the configuration of atomic electrons do not differ substantially from the data base available to Lotz. Comparison with the more recently expanded base of measured data shows that re-appraisal of the Lotz fitting parameters is required at least for lowly charged ions of dominant impurity species (see the typical case of $Fe^{+} \rightarrow Fe^{2+}$ shown in Figure 16).

. For each ionisation cross section needed for plasma modelling there are many excitation cross sections which must describe the dominant excitation processes experienced by an ion in each of its charge states. The requirement for a very wide base of data has motivated the search for a simple treatment of excitation cross sections and the most frequently employed methods are based on the Bethe approximation. The wave length of high energy electrons is much smaller than atomic dimensions and this causes the dominant interactions to occur outside the range of the atom wave functions. In effect the influence of the charge of the incident electron upon the atomic electron can be neglected and for, these long range collisions, the interaction potential operator [see Eq. (6.8)] becomes equal to the absorption oscillator strength of the atomic electron. The high energy collision can thus be regarded as a radiative process in which (a) the incident electron enters the electric field due to the atomic electron, (b) the incident electron then emits a photon and (c) this photon is absorbed by the atom and gives rise to a transition $o \rightarrow n$. The semi-empirical approach which has evolved from this concept[27,28,29] is usually referred to as the Gaunt factor (or g) formula and it takes the form

$$\sigma_{on} = \frac{8\pi}{\sqrt{3}} \left(\frac{E_{i,H}}{E_{on}}\right)^2 \left(\frac{E_{on}}{E}\right) f_{on} \bar{g} \left(E_{on}/E\right) \pi a_o^2 \qquad (6.22)$$

where f_{on} is the absorption oscillator strength and $\bar{g}$ an empirial form of the Kramers-Gaunt $\bar{g}$ factor[30]. There is considerable doubt

regarding the selection of $\bar{g}$. The limited amount of experimental data (Refs. 31,32,33,34) indicate that $\bar{g} \sim 1$ for $\Delta n = 0$ transitions in ions of charge state greater than $z \sim 5$ and in addition $\bar{g}$ tends to be invariant with E. (This trend is also supported by theory). For more lowly charged ions $\bar{g} \to 0.2$ at low energies and moreover it displays a dependence upon (E/E_{on}). In cases where $\Delta n \neq 0$, there are indications that $\bar{g}$ is less than 0.2. Dunn[33] cautions that the $\bar{g}$ formula is likely to be accurate only to a factor two or three.

6.3 Experimental Methods

In order to measure absolutely the cross section for a collision between an incident particle (A) and a target particle (B) it is necessary to know the densities n_A and n_B of the particles and to measure the rate ν_{AB} at which collisions occur within a well defined volume V. The cross section at a collision energy E corresponding to a collision velocity v_o is given by

$$\sigma(E) = \frac{\nu_{AB}}{n_A n_B V v_o}. \qquad (6.23)$$

Collision rates are determined by observing the absolute rate of formation of collision products (A' and B') and this is most readily achieved if the collision changes the charge state of the particle. For example, the B' product ions which are formed by electron impact ionisation in the reaction

$$e + B^{z+} \to e + e + B^{(z+1)+} \qquad (i)$$

or by charge exchange in the reaction

$$A^+ + B \to A + B^+. \qquad (ii)$$

The neutral A' products of the incident A^+ atoms in reaction (ii) are also readily detected if their energies are in excess of a few hundred electron volts. Product photons are much more difficult to observe in a meaningful manner. Firstly, photon emission may be angularly distributed relative to the collision velocity vector $\vec{v}_o$. Secondly, wavelength resolution is required and this severely reduces the fraction of product photons that can be detected.

Many cross section measurements are based upon the principles of the beam-static target technique. In this method a monoenergetic beam of flux I_A (type A particle/s) is directed through a thermal gas target of uniform density n_B. The cross section is determined from the expression

$$\sigma(E) = \frac{\nu_{AB}}{I_A} \frac{1}{l n_B} \qquad (6.24)$$

where ν_{AB} is the absolute rate of production of B' products (and

less generally A' products) within a well defined length l of the beam. The line density ($l n_B$) is maintained at a small value in order that multiple collisions can be neglected. This method has yielded data for electrons, ions and atoms incident upon (a) rare gas targets and (b) molecular gas targets. To apply the technique to ions or atoms incident upon atomic hydrogen the target cell (which for such measurements is made from tungsten) is heated to a temperature in excess of 1800 K in order to dissociate virtually all of the H_2 molecular gas.

Studies of collisions which involve atomic oxygen have been performed by replacing the gas cell by a beam of thermal energy oxygen atoms which is formed by allowing atoms to effuse through a small hole in the wall of a radio-frequency discharge tube. Beams of atomic hydrogen are also formed by atom effusion from a hot tungsten furnace which is fed with molecular hydrogen. This technique of thermal atom beams crossed with electron (or ion) beams was pioneered by Fite and his colleagues (see for example Ref. 35) and it has been used for studies of electron impact ionisation and excitation and also proton and O^+ charge exchange. The density of particles in the beams is appreciably less than in the static gas cell, indeed it is frequently smaller than the density of residual gas in the apparatus. Beam modulation techniques are used to distinguish the signals (i.e. amplified currents of ions or photons which arise from ν_{AB}) from the larger backgrounds due to collisions of the incident particles with residual gas.

Cross sections for collisions between electrons and ions, ions and ions and in some cases electrons and ground state or excited atoms are measured using fast colliding beams. The term fast is used to distinguish these target ion beams of 1 to 20 keV energy from the thermal energy atom beams. Fast neutral beams are produced by charge exchange in a gas or vapour cell (see Figure 11). The fast beam technique which was pioneered by Dolder and Harrison and their colleagues (see for example Ref. 36) is the main source of cross section data for ionisation and excitation of impurity ions and also for electron collisions with H_2^+. The target beam density is considerably smaller than in thermal beam experiments (ranging from 10^3 to 10^6 type B particles/cm^3) and quite sophisticated beam pulsing techniques are used to distinguish the count rates of particles which arise due to beam collisions from those which arise due to collisions with residual gas or surfaces within the apparatus. Fast beam techniques offer a number of advantages; the detection efficiency of both charged and neutral particles is high and absolute measurements can be made. Coincidence counting of the A' and B' products can also be used to further distinguish the collision process. Unfortunately the technique offers little scope for studies of molecules because, unlike atoms, fast neutral molecules are not readily formed by charge capture.

The angle of intersection of the beams can be varied in order to attain a low or high collision velocity within the centre of mass frame whilst retaining a high velocity within the laboratory frame. The angle of intersection ranges from $\phi \to 0$ (merged beams), to $\phi = 5^{o}$ to 20^{o} (inclined beams) and to $\phi = 90^{o}$ (crossed beams). These various configurations are illustrated in Figure 11. The scanning shutters S shown in Figure 11 are used to measure the current density distributions in both of the beams because the assumption, implied in Eq. (6.24) that the target density n_B is uniform is not valid when the target is a fast beam. The fast colliding beams method has, to date, been restricted to target ion charge states z less than 5. Measurements of excitation cross

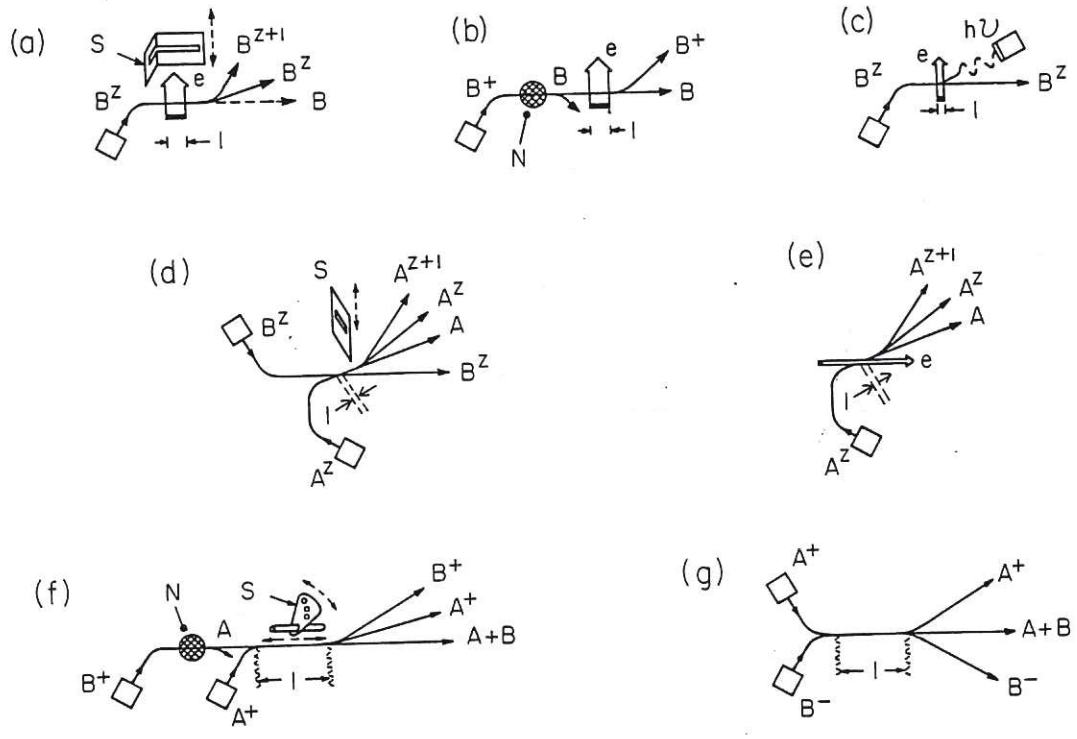

Fig. 11 Configurations used in colliding beam experiments. (a) Crossed electron-ion beam, (b) crossed electron-fast atom beams, (c) crossed electron-ion beams used for excitation studies, (d) inclined ion-ion beams, (e) inclined electron-ion beams, (f) merged ion-atom beams and (g) merged positive and negative ion beams. S is a shutter used to measure the profiles of current densities (and hence the profiles of particle densities), N is a neutraliser gas cell in which target atoms are formed by charge capture and l is the length of the collision path. For details see Harrison (Ref. 37).

sections for ions are particularly difficult because of the low density of the fast target beam and the low overall efficiency of wave-length selective detectors for photons in the far ultra-violet and soft X-ray region of the spectrum.

There are many reviews of experimental measurements. Kieffer and Dunn[38] have surveyed beam-static target experiments and early crossed beams experiments. Recent studies of inelastic collisions of electrons with ions are reviewed in Refs. 31, 32, 33 and 34 and these papers also provide bibliographies of earlier but pertinent review articles. Recent reviews of experimental methods used in charge exchange measurements have been provided by de Heer[39].

7. MEASURED DATA FOR ELECTRON IONISATION AND EXCITATION

The measured cross section for ionisation of the ground state hydrogen atom is shown in Figure 12. It displays the high energy dependence predicted by the Born approximation but at lower energies the agreement with quantum theory is less satisfactory. The cross section recommended by Bell et al.[40] is derived from a

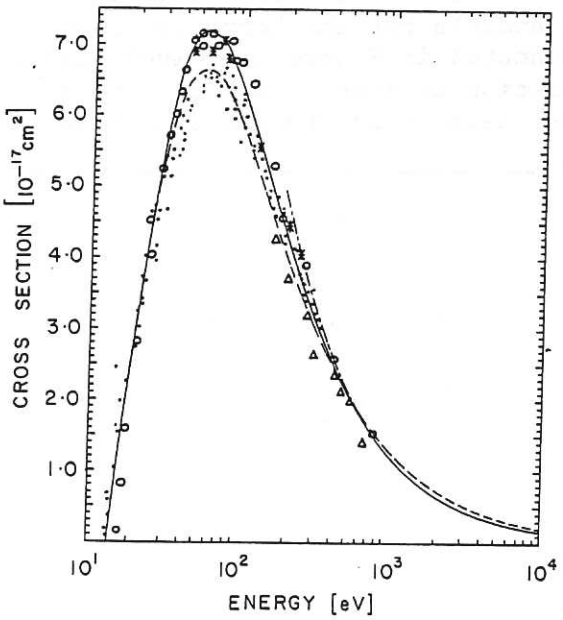

Fig. 12 Cross section for $e + H(1s) \rightarrow 2e + H^+$.
Data taken from an assessment by Bell et al. (Ref. 40).
The solid line is the cross section recommended in Ref. 40 and the dashed line is the semi-empirical Lotz cross section calculated using Eq. (6.21).
The open circles are the measured data of Fite and Brackmann[35]. Other symbols are described in Ref. 40.

critical appraisal of both experimental and theoretical data.

The scaling relationship expressed in Eq. (6.3) is well demonstrated by the comparison of the scaled ionisation cross section for atomic hydrogen with the isoelectronic ion He^+ which can be seen in Figure 13. The ionisation threshold energies of these simple one electron atomic species scale as $(E_{iH}/E_{iHe^+}) = Z^{-4}$ where Z is the atomic number. Consequently the magnitude of the cross section of He^+ ion is expected to be 16 times smaller in magnitude than that of the H atom. This relationship holds well at incident energies in excess of $(E/E_i) \gtrsim 5$ but not at lower energy. The reason is that during an electron-ion collision the incident electron enters the relatively long range Coulomb field of the nucleus and it is thereby accelerated. Interchange of energy with the bound electron takes place only after the incident electron has experienced some degree of acceleration and, as a consequence, there is a greater probability of imparting energy to the bound electron. This causes the ionisation cross section for ions to be more peaked in the low energy regime. The trend is quite general and has prompted comparison of data along isoelectronic sequences so that differences in the screening of the nucleus by the bound electrons in partially stripped ions are minimised. An example for the beryllium sequence taken from Bell et al.[40] is presented in Figure 14. Such scaling should be applied with caution because indirect contributions to the total ionisation cross section by processes such as excitation of

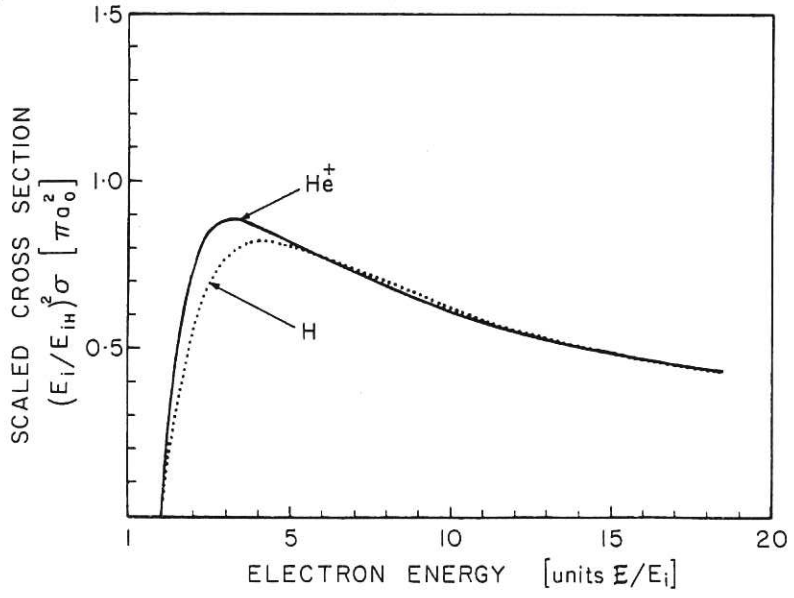

Fig. 13 Comparison of the measured cross sections for $e + H(1s) \rightarrow 2e + H^+$ and $e + He^+(1s) \rightarrow 2e + He^{2+}$. Data for H(1s) are from Fite and Brackman[35] and those for $He^+(1s)$ are from Dolder et al. (Ref. 36).

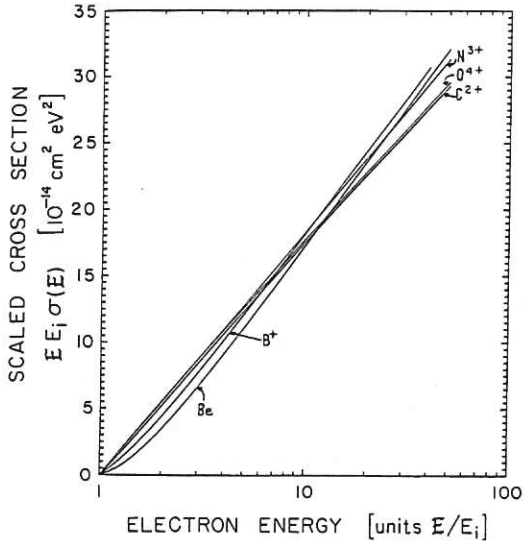

Fig. 14 Scaled cross section for ionisation of beryllium like ions.
Data taken from Bell et al. (Ref. 40).

autoionising transitions do not scale with ionic charge state z in such a simple manner (see for example Crandall[31]).

Simple scaling based upon the energy levels of the Bohr atom implies that the ionisation cross section of excited hydrogenic species will scale as $\sigma_n(E/n^2) \propto n^4\sigma_o(E)$. Thus the cross section for H(2s) at the scaled energy (E/n^2) is expected to be about 16 times larger than that of the H(1s) ground state atom. Measured data are presented in Figure 15 and comparison with the H(1s) cross section shown in Figure 12 shows that there is reasonable support for such scaling.

Attention has already been directed in Section 4.3 to the existance of a multiplicity of interactions which can contribute to the total ionisation cross sections of multi-electron atoms and ions. A typical and relevant example of such effects is portrayed by the ionisation process $e + Fe^+ \rightarrow e + e + Fe^{2+}$ whose cross section appears in Figure 16. Comparison of the measured data with the scaled plane-wave-Born approximation of McGuire[43] for the outer and inner shell electrons clearly demonstrates that inner shell ionisation is the dominant process.

The somewhat similar energy dependence of the cross sections for ionisation and for excitation of an allowed transition is demonstrated in Figure 17 by the cross section for excitation of (1s to 2p) transitions in atomic hydrogen. Also shown is the

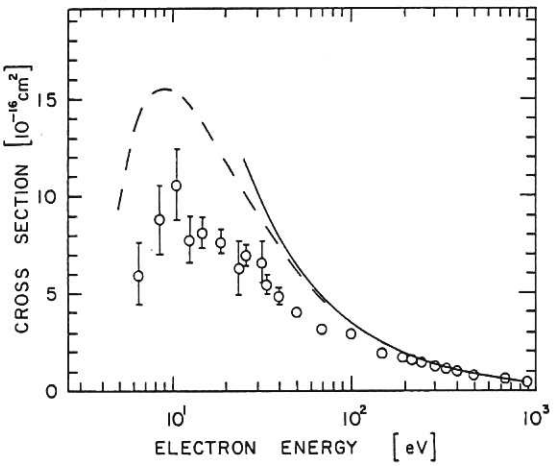

Fig. 15 Cross section for ionisation of metastable H atoms ($e + H(2s) \rightarrow e + e + H^+$).
Experimental data are taken from Defrance et al. (Ref. 41). The solid curve is a Bethe approximation calculation and the dashed curve a Born approximation calculation.

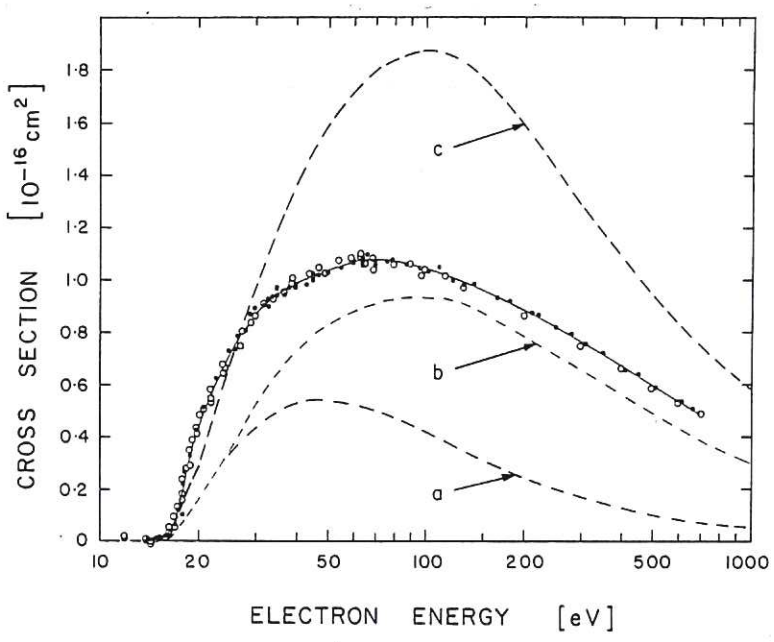

Fig. 16 Cross section for $e + Fe^+ \rightarrow 2e + Fe^{2+}$.
Data from Montague et al. (Ref. 42). Curves (a) and (b) are respectively scaled Born approximations (Ref. 43) for outer and for outer plus inner electrons, (c) is the Lotz cross section.

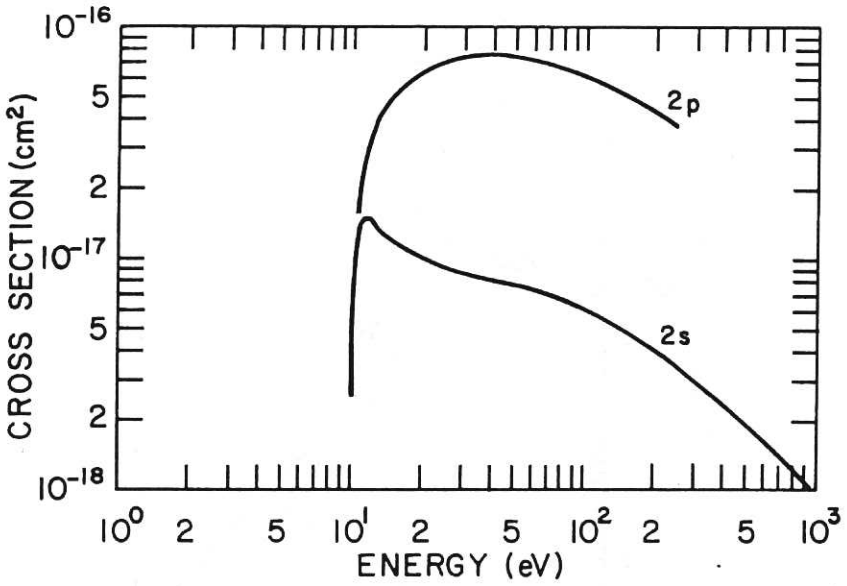

Fig. 17 Excitation cross sections for e + H(1s) → e + H(2p) and e + H(1s) → e + H(2s) [plus cascade contributions from upper levels to the 2s level].
Data are taken from the compilation by Barnett et al. (Ref. 44).

cross section for excitation of the disallowed transition (1s to 2s) which has a markedly different energy dependence. The very strong energy dependence of cross sections for excitation of a disallowed transition which also involves a change in multiplicity are shown in Figure 18. The data are for excitation of 1^1S ground state helium atoms to the 4^3S and 4^3P states. For comparison, data for allowed transitions to the 3^1P state are also shown.

The low energy dependence of the excitation cross section of an ion differs significantly from that of an atom. The difference is attributable to the requirement that total angular momentum must be conserved within the collision system. Consider an incident electron whose energy at infinite separation from the atom is exactly equal to the threshold (E_{on}) corresponding to an electron transition which produces a precise change in angular momentum [$\ell_{on}(h/2\pi)$] of the atom. This electron is brought to rest when it excites the atom so that it has zero angular momentum after the collision. In order to conserve the total angular momentum of the system, the incident electron [whose velocity must be $v_e = \sqrt{2E_{on}/m_e}$] is allowed only one specific value of impact parameter. However, a free electron is entitled to have an infinite number of impact parameters; consequently the excitation

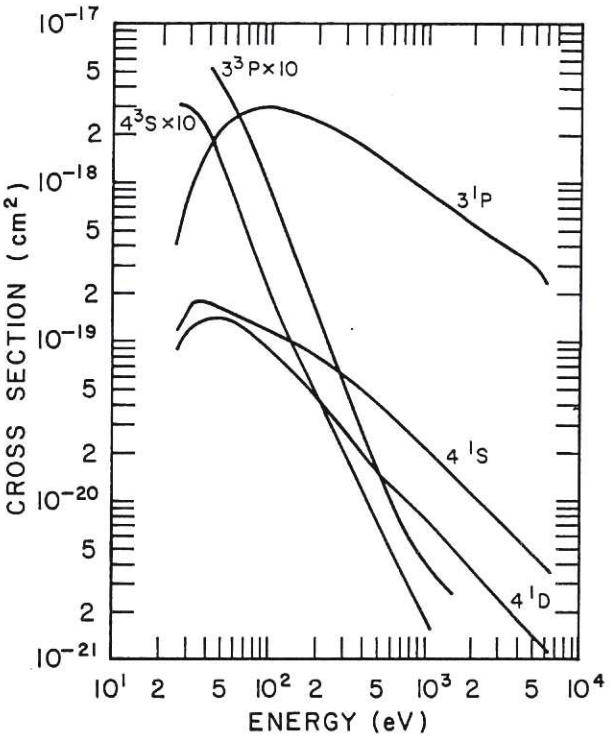

Fig. 18 Cross sections for e + He → e + He (4^1S; 3^1P; 4^1D; 4^3S, 3^3P).
Data are taken from the compilation presented in Ref. 44.

cross section of the atom becomes infinitely small when $E \to E_{on}$. This constraint is removed when the electron collides with an ion because prior to the interaction the incident electron enters the Coulomb field of the ion and is accelerated to energies in excess of E_{on}. As a consequence, excitation of the ion does not bring the electron to rest and so the mobile scattered electron can carry away any angular momentum which is surplus to the collision. Electron impact excitation cross sections of ions are actually finite at energies immediately above the threshold. This can be seen clearly in the measurement of the excitation cross section of the $He^+(1s \to 2s)$ transition which is shown in Figure 19.

The abrupt onset of excitation is also evident in the excitation of autoionising transitions in ions. Evidence of the effect is apparent in the total ionisation cross sections shown in Figure 20. In certain cases (e.g. Ba^+) contributions from autoionisation are the dominant ionisation process. Burgess and Chidichimo[46] have taken account of auto-ionisation in an empirical manner and have proposed an expression for the total ionisation of ions whose charge state exceeds z = 2.

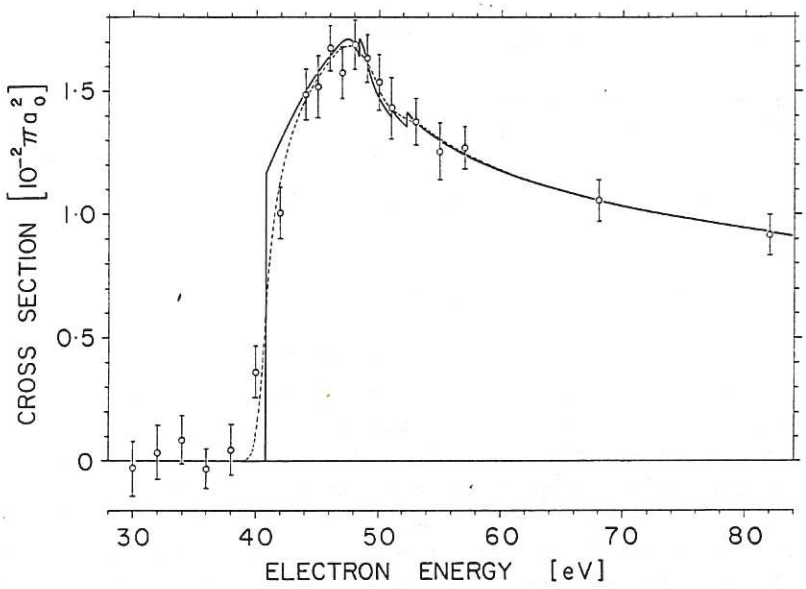

Fig. 19 Cross section for e + He^+ (1s) → e + He^+ (2s) [plus cascade contributions to the 2s level].
Data from Dance et al. (Ref. 45).

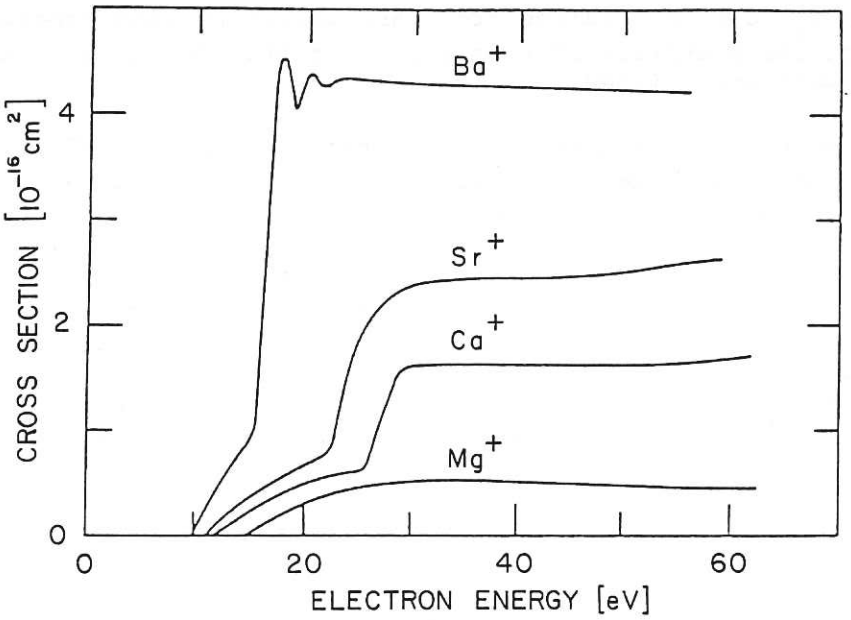

Fig. 20 Measured cross sections for electron impact ionisation of Mg^+, Ca^+, Sr^+ and Ba^+.
Data taken from the review by Dolder (Ref. 34).

8. ELECTRON COLLISIONS WITH MOLECULES

The principles of collision physics outlined in Section 9 are applicable but the electronic charge distribution of the molecule is more complex. This can readily be appreciated from the wave equation of a molecule in a electronic state n and vibrational state υ, namely

$$\Psi_{n\upsilon JM} = \phi_n(r_e R)\,\chi_{n\upsilon}(R)\,\rho_{JM}(\Theta\phi) \qquad (8.1)$$

Here J and M are the rotational quantum numbers (it being assumed that the contribution due to nuclear rotation around the molecular axis is zero), r_e denotes the coordinates of the molecular electrons relative to the nuclei, R is the nuclear separation and Θ and ϕ are the polar angles of the nuclear axis relative to a fixed position in space (for example the direction of the incident electron). The term ϕ_n gives rise to the electronic energy $E_n(R)$, shown for H_2 by the curves in Figure 6, and the other terms account for vibrational and rotational states.

In the case of neutral molecular hydrogen there exists a substantial amount of measured data for excitation and also for the various collisions (discussed in Section 5.2) which give rise to either H_2^+ or H^+. There are but sparse data for the important process of dissociation into (H + H) atoms because in these measurements it is rather difficult to detect the low energy H atoms. Data for H_2^+ can be obtained from fast colliding beam experiments and, with the exception of photon production, the measured data base is well established.

It must be reiterated that H_2^+ which arises from electron impact upon H_2 will be formed in a distribution of vibrationally excited states (see Section 5.1) and the cross sections for both excitation and ionisation increase strongly with increasing υ. The effect can be seen in Figure 21 which shows the measured cross section for the production of H^+ in electron collisions with H_2^+. It is evident that the cross section increases with decreasing electron energy in the low energy regime below the threshold corresponding to the $\upsilon = 0$ ground vibrational state. However it seems reasonable to assume that the vibrational population in the plasma edge can be determined by the appropriate Frank-Condon factors given by Dunn[48]. Somewhat similar populations are likely to exist in crossed beams experiments so that the existing base of measured data is reasonably applicable to the edge plasma. When applying theoretical data for H_2^+ collisions it is necessary to ensure that the data correspond to the appropriate distribution of vibrational states (see the discussion in Harrison[3]).

A concise but comprehensive survey of electron collisions

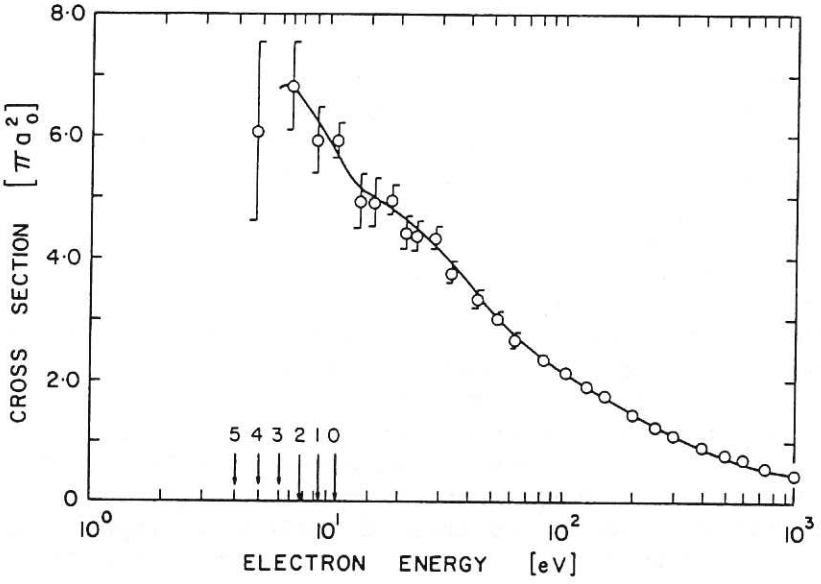

Fig. 21 Cross section for production of protons by electron impact on H_2^+.
Data taken from Dance et al.[47] The cross section corresponds to [reactions (26+27) + twice reaction (28)]. The threshold energies from the v = 0, 1, 2, 3, 4 and 5 vibrational levels are shown.

with neutral and ionised H_2, D_2, T_2 together with some simple hydrocarbons can be found in de Heer[49].

9. COLLISIONS BETWEEN HEAVY PARTICLES

This category embraces collisions between two particles each of which have bound electrons or, in the case of a fully stripped ion, can capture an electron into a bound state. The consequences of the collision can be the exchange of one or more electrons between the particles (i.e. electron capture), the ejection of bound electrons (ionisation of the target or stripping of an energetic incident particle), direct excitation of the electronic states of the particles and indirect excitation which arises due to electron capture into excited states. When the colliding particles are widely separated each has the electronic charge distribution of the individual atomic species but as the particles approach each other these distributions may overlap and the collision system can be considered as a transitory molecule. After the collision, the product species move apart and each of them take up the characteristics of individual atomic species. It is therefore

convenient, especially at low collision velocity, to model the collision on the concept of transitions between the states of the molecules which describe the collisions partners before and after their interaction. The internuclear separation is here related to the distance between the colliding particles and the time during which the transitory molecule exists i.e. the collision time, t_{coll}, is related to the collision velocity and the dimension of the system. Except at very high collision velocities, the wave length of the incident heavy particle is appreciably larger than the dimensions of the collision system and the particle trajectories can therefore be described by classical mechanics but the transitions which involve the bound electrons must be treated by quantum theory. This is in contrast to electron collisions where the impact parameter must be quantised because of the short wavelength of the incident electron. At high velocities quantum theory must also apply to heavy particle collisions. Indeed, when $E > 100$ keV, the cross sections for proton impact ionisation and excitation are similar to those for electron impact collisions at the same velocity and can be well described by the Born approximation.

At such high energies the collision time is much shorter than the time required for transitions between the states of the transitory molecule so that molecular effects tend to be insignificant. However, when the particles move slowly, the electronic transition time ($t_e \sim h/\Delta E$ where ΔE is the difference in potential energy between the molecular states) can be much less than the collision time $t_{coll} = a/v$. Here a is the range of the collision which can be related to molecular dimensions (typically 2 to 3 Å) and v is the collision velocity. At low collision velocity the transfer of momentum to the bound electrons is insufficient for direct excitation and ionisation so that collisions in this regime are predominantly related to charge exchange interactions of the type

$$A^+ + B \rightarrow A + B^+ + \Delta E. \qquad (30)$$

Here ΔE is the difference in potential energy between the left hand and right hand sides of reaction (39) and it can be either positive (exothermal) or negative (endothermal). In either case the imbalance is transferred into a change in kinetic energy of the colliding particles.

Recent reviews of the theories which are appropriate to the various regimes of heavy particle collisions have been provided by Brandsden[50] and a critical appraisal of theoretical data for charge exchange between H atoms and highly charged ions can be found in Janev and Brandsden[51]. A critical survey of experimental data for both electron capture and ionisation during collisions with hydrogen is also available (Gilbody[52]). Both experimental and theoretical data have been reviewed by de Heer[39] who also

discusses the experimental methods employed.

9.1 Electron Capture by Singly Charged Ions

If the presence of non-thermalised energetic particles is neglected then the upper limit of collision energies in the edge plasma is only a few hundred electron volts so that direct ionisation and excitation tend to be insignificant in collisions between heavy particales. Charge capture from recycling hydrogen atoms is important and it is therefore the main topic of the following discussion. For the sake of conciseness interactions involving hydrogen molecules and negative ions are not considered. A brief survey of molecular processes which are likely to be significant in the edge plasma can be found in Janev et al[8].

In the case of low-energy collisions Massey[53] has postulated that any perturbations of the molecular states caused by the collision will have little effect (because the perturbation frequency cannot resonate with the transition frequency) whenever the collision time, t_{coll}, is substantially greater than t_e. The implication of this adiabatic criterion is that the cross section for the collision is small if

$$a|\Delta E|/hv >> 1 \qquad (9.1)$$

Other workers, notably Hasted[54], have invoked the corollary of the aidiabatic criterion (namely the diabatic condition) which infers that a charge exchange cross section reaches its peak at a velocity $\hat{v}$ given by

$$\frac{a}{\hat{v}}\left(\frac{\Delta E}{h}\right) = 1 \qquad (9.2)$$

According to Eq.(9.2) the peak occurs at a collision energy $\hat{E}$ given by

$$\hat{E} = 36|\Delta E|^2 m_i a^2 \quad [eV] \qquad (9.3)$$

where m_i is the mass (in units of the electron mass m_e) of the incident particle and a is in units of a_o. A typical example of this condition is the cross section for the reaction

$$He^+(1s) + H(1s) \rightarrow He(1s^2) + H^+ + (11\ eV) \qquad (31)$$

which is shown in Figure 22. The value of $\hat{E}$ is about 20 keV/amu which is consistent with Eq.(9.3). At collision energies below $\hat{E}$, the interaction is increasingly adiabatic and the cross section may have the form

$$\sigma_{cx} \approx A \exp(-B\Delta E/hv) \qquad (9.4)$$

where A and B are constants. At energies $E > \hat{E}$ the collision time becomes small and the cross section decreases with increasing collision energy as can be seen in Figure 22.

Clearly the case of symmetric, resonant charge exchange is a special case and the simplest of such reactions,

$$H^+ + H(1s) \rightleftarrows H(1s) + H^+ + (\Delta E = 0) \qquad (32)$$

plays many roles in fusion research. Because the reaction is energy resonant Eq. (9.2) retains physical significance only when $\hat{v} = 0$ and this implies that the cross section is a maximum at zero collision energy. The measured data, which clearly demonstrate this characteristic, are shown in Figure 23. The adiabatic condition becomes progressively less relevant with increasing collision energy and the theoretical cross section determined by a semiclassical impact parameter treatment, has the form

$$\sqrt{\sigma_{cx}} = a - b \ln v \qquad (9.5)$$

where a and b are constants. The curve, which is fitted to the measured data in Figure 23, demonstrates this type of energy dependence.

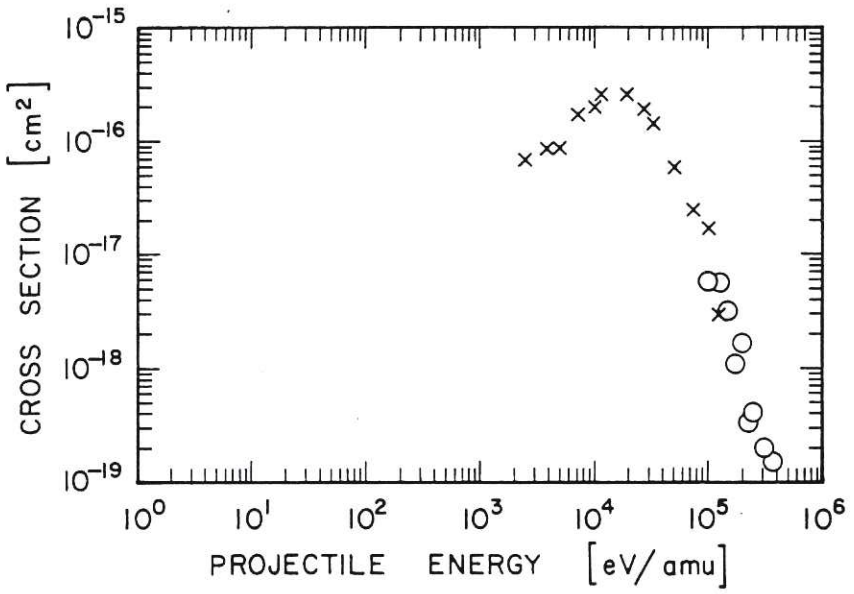

Fig.22 Cross section for $He^+(1s) + H(1s) \rightarrow He(1s^2) + H^+$. The circles show measured data of Olson et al.[55] and the crosses measured data of Hvelplund and Andersen (Ref. 56).

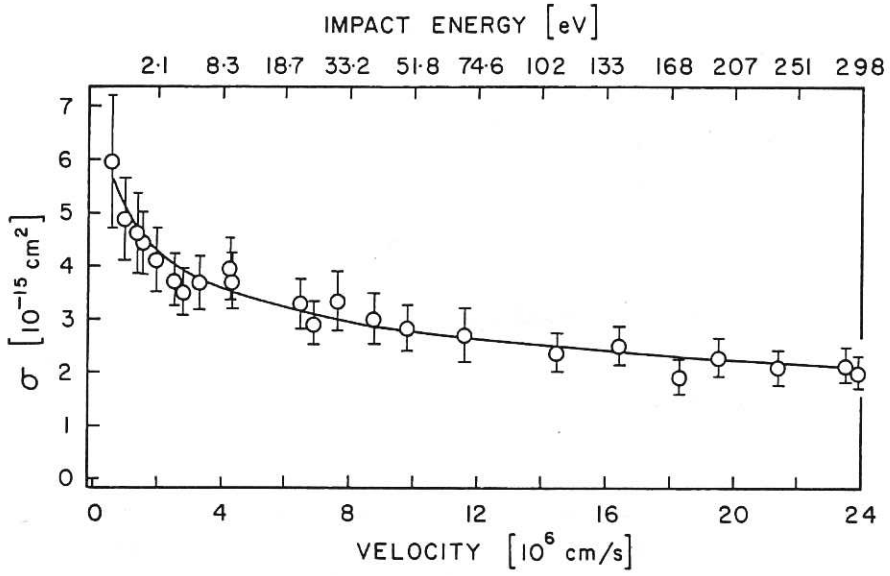

Fig. 23 Cross section for $H^+ + H(1s) \rightleftarrows H(1s) + H^+$
Experimental data are from Newman et al.[57]. The fitted curve is based upon the expression
$\sigma_{cx} = (7.07 - 1.83 \log_{10} v)^2$ which is given by Greenland (Ref. 58).

Collisions involving dissimilar particles are not in general energy resonant but there are many examples of accidental resonance. Some are of relevance to the boundary plasma and one such is

$$O^+(^4S) + H(1s) \rightarrow O(^3P_J) + H^+ \qquad \begin{cases} -\ 0.01\ \text{eV}\ (J=0) \\ +\ 0\ \text{eV}\ \ (J=1) \\ +\ 0.02\ \text{eV}\ (J=2). \end{cases} \qquad (33)$$

The characteristics of resonant charge capture are clearly evident in the measured cross section shown here in Figure 24. However this cross section is smaller than the symmetric resonant case of $H^+ + H$. The difference can be ascribed to the fact that H(1s) has only a single level and so each H(1s) interaction with H^+ has a zero energy defect. By contrast the levels of the atomic species involved in the capture process $O^+ + H$ are multiple so that $\Delta E \sim 0$ is not valid for transitions between some sub-levels. Thus it is necessary to weight the electron capture probability by a factor which is less than unity and which is related to the statistical weights of the atomic systems involved in both the forward and the reverse direction of the collision process. The reverse reaction ($H^+ + O$; Ref.60) exhibits the same energy dependence but its magnitude is smaller by a factor of about 8/9.

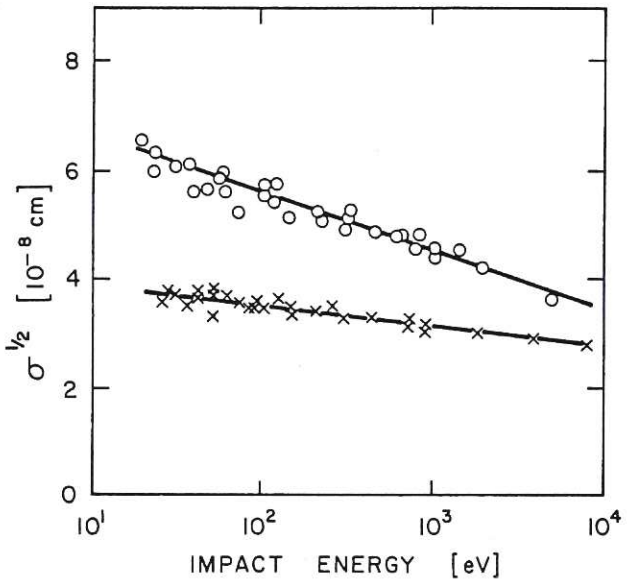

Fig. 24 Measured cross sections for $H^+ + H \rightarrow H + H^+$ and for $O^+ + H \rightarrow O + H^+$.
Data taken from Ref. 59; the circles refer to H^+ and the crosses to O^+.

9.2 Charge Exchange Involving Multiply Charged Ions

It will be noted that for reactions (31), (32) and (33) the value of ΔE has been taken to be equal to the difference between the potential energy of the isolated atomic species. For this assumption to be valid, the value of ΔE must tend to be independent of the internuclear separation so that $d\Delta E/dR \rightarrow 0$. The molecular potential energy curves which describe many collisions involving singly ionised ions and neutral particles tend to display this characteristic and a typical case for $He^+ + H$ is shown in a qualitative manner in Figure 25(a). There are however cases where ΔE varies strongly with R and this is most evident in collisions in which both particles are ionised and therefore experience Coulomb repulsion either before or after the interaction. Typical examples of such collisions are:

$$A^{(z+1)} + B \rightarrow A^{z+} + B^+ + \Delta E(R) \qquad (34)$$

or

$$A^{z+} + B^+ \rightarrow A^{(z+1)+} + B + \Delta E(R) \qquad (35)$$

where $z \geq 1$. The potential energy curves for these reactions are of the form shown qualitatively in Figure 25(b). The intersection

of the curves occurs at

$$R_c \approx (z-1)/\Delta E \qquad (9.6)$$

where ΔE is the value at infinite separation. The parameters in Eq. (9.6) are in atomic units (a u), namely length in a_o, z in units of the electronic charge e and the unit of energy is ($2 \times E_{i,H} = 27.21$ eV). It is clear that charge exchange is most

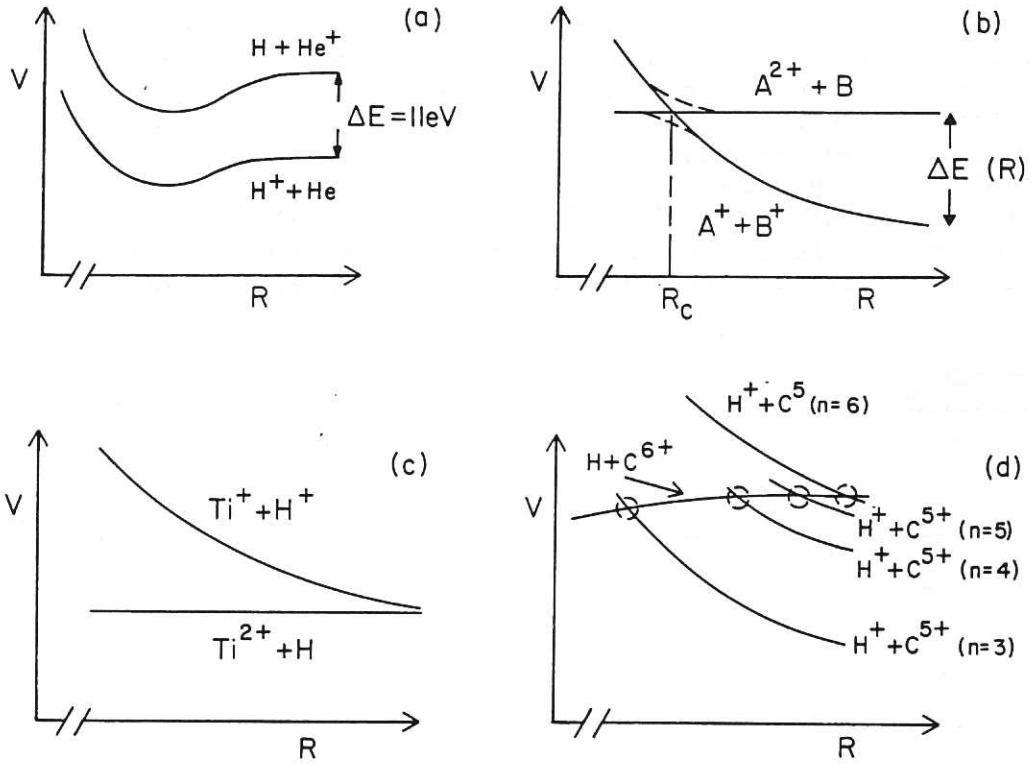

Fig. 25 Qualitative representations of potential diagrams for charge exchange collisions.
(a) $He^+ + H(1s) \rightarrow He(1s^2) + H^+$

(b) Curve crossings
Psuedo crossings are indicated by the dashed adiabatic curves and crossings by the solid diabatic curves.

(c) $Ti^+ + H^+ \rightarrow Ti^{2+} + H$

(d) $H + C^{6+} \rightarrow H^+ + C^{5+}$

likely to take place at internuclear separations around R_c so that the maximum cross section will be of order

$$\hat{\sigma}_{cx} \sim \pi R_c^2. \tag{9.7}$$

At low collision energy, and hence within the adiabatic regime, the initial (i) and final (f) states correspond to those of a steady state molecule so that the non-crossing rule (Wigner and Witmer[61]) requires that the potential curves of states with the same symmetry do not cross. Thus the adiabatic potentials are of the form indicated by the dashed curves in Figure 25(b) and only psuedo-crossings can occur. At higher energies (in the diabatic regime) a jump is possible between the potentials curves and so the solid (diabatic) curves apply. The energy defect ΔE becomes small when $R \to R_c$ and it is evident from Eq.(9.3) that $\hat{E}$ is much smaller than in cases where no crossing or psuedo crossings take place. In the low velocity regime ($v < 1$ au, i.e. less than 2.2×10^8 cm/s) where the molecular aspects of the collision dominate, the Landau-Zener theory[62] has been applied for transitions between levels of the same symmetry. According to this approach the diabatic condition Eq.(9.2) is modified to take the form

$$\frac{a' \, \Delta E(R_c)}{h \, \hat{v}} = 1 \tag{9.8}$$

where

$$a' = \frac{\Delta E(R_c)}{\frac{d}{dR} (V_i - V_f)_{R = R_c}} \tag{9.9}$$

and

$$\Delta E(R_c) = 2 \, H_{if}. \tag{9.10}$$

Here H_{if} is the matrix element for the coupling of the diabatic states. The denominator in Eq.(9.9) is the difference in the slopes between the diabatic potential curves (V_i and V_f) at R_c. Such calculations take note of the fact that the particles must pass through R_c as they approach each other and also as they separate after the collision.

The reactions

$$Ti^+ + H^+ \to Ti^{2+} + H + (\Delta E \approx 0) \tag{36}$$

and

$$Fe^+ + H^+ \to Fe^{2+} + H + (\Delta E \approx 2.4 \text{ eV}) \tag{37}$$

which are shown in Figure 26 are relevant examples of the effects

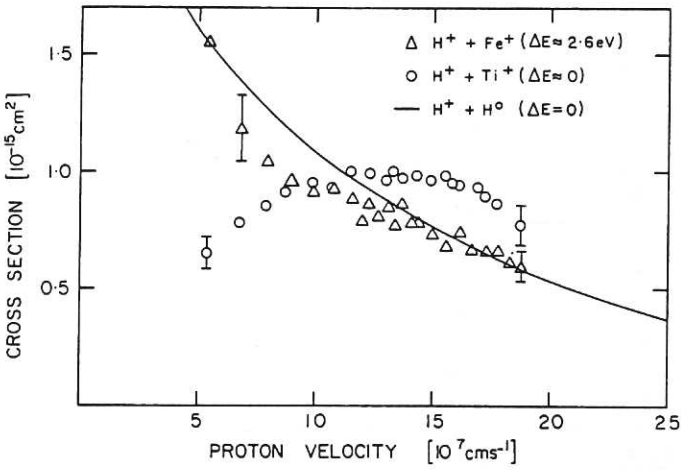

Fig. 26 Measured cross sections for the production of doubly charged ions in collisions between protons and Ti^+ and also Fe^+ ions. Data which are taken from Ref. 63 relate predominantly to charge capture by protons.

of variation of ΔE with R. The $Ti^+ + H^+$ collision for which $\Delta E \approx 0$ at infinite separation exhibits the characteristic of a non-resonant interaction because the potential energy curves are expected to be of the form shown in Figure 25(c). In contrast, the $Fe^+ + H^+$ collision tends to display resonant behaviour which indicates that the value of ΔE at R_c must be very much smaller than ΔE at infinite separation.

The ionisation potential of a multiply charged ion A^{z+} always exceeds that of any neutral collision partner so that capture into an excited state of the $A^{(z-1)*}$ ion is a likely event. One of the simplest reactions is

$$He^{2+} + H(1s) \rightarrow He^+(n=2) + H^+ + (\Delta E=0). \qquad (38)$$

However this cross section is small in the aidiabatic regime because the Coulomb repulsion between the He^+ and H^+ ions causes the potential curves to take a form comparable to that shown for $Ti^+ + H^+$ in Figure 25(c). However, in the case of higher charge states, the number of available excited states becomes larger and multiple curve crossings, such as those shown for $H + C^{6+}$ in Figure 25(d), can contribute significantly to charge exchange. In this particular interaction the partners $[H + C^{5+}(n=6)]$ have $\Delta E = 0$ at infinite separation but the charge exchange interaction is expected to be dominated by the $[H + C^{5+}(n=4)]$ partners. The effect of such multiple crossings is to flatten the peak of the cross section. As the ion charge state increases more and more curve crossings are involved and the weaker becomes the velocity

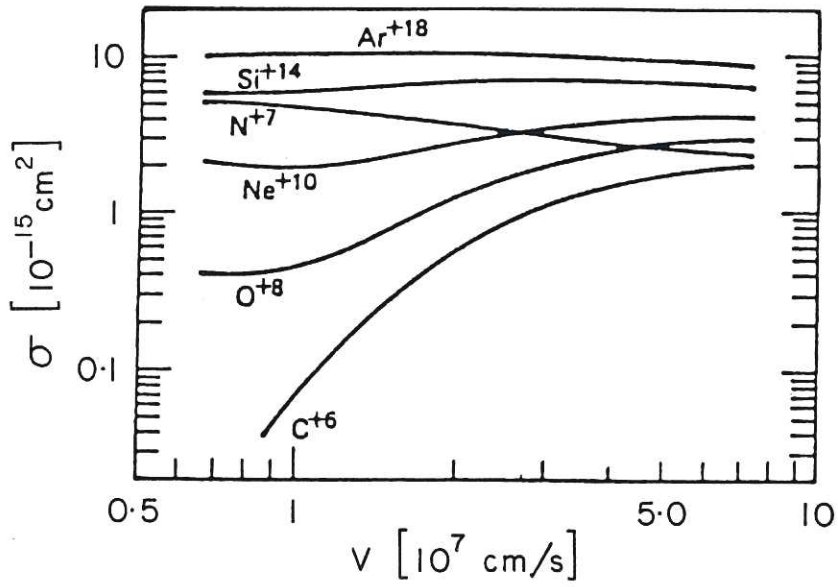

Fig. 27 Total Landau-Zener cross sections for charge exchange between H(1s) atoms and various stripped ions. Data taken from Salop and Olson (Ref. 64).

dependence of the cross section. The trend, as predicted by the Landau-Zener theory, is illustrated in Figure 27 and there are experimental data (see the reviews in Refs. 39 and 52) which support this characteristic behaviour. Greenland[58] has compiled and assessed data for low energy charge exchange between H atoms and multiply charged ions of particular relevance to the plasma edge. He also provides convenient analytical expressions for these cross sections.

In the region of low velocity (i.e. $v < 1$ au) and low charge state ($z \leq 4$) there are relatively few curve crossings especially in collisions which involve simple atomic systems such as fully stripped ions and/or H atoms. The electron capture cross sections are then strongly dependent upon the detailed structure of the molecular potentials and so no simple scaling with ion charge state can be established. However, for collisions involving non-hydrogenic atoms and/or partially stripped ions, the number of crossings increases very strongly with z and the collision range [R_c in Eq. (9.6)] can be considered to vary continuously with z. Indeed the number of crossings and hence collision channels becomes so great that electron capture can be regarded as the decay of the initial electronic state into the quasi-continuum of final ionic states and so the binding energy of the initial state can also be related to z. Janev and Hvelplund[65] propose (for ions with $z \geq 5$) a scaling relationship based upon a reduced charge exchange cross section ($\tilde{\sigma}_{cx} = \sigma_{cx}/z$) and a reduced velocity ($\tilde{v} = vz^{-1/4}$). The scaling is

$$\tilde{\sigma}_{cx} = \sigma_{cx}(\tilde{v})\ z^{\alpha(\tilde{v})}. \qquad (9.11)$$

Curves of $\tilde{\sigma}_{cx}$ versus reduced collision energy ($\tilde{E}/\sqrt{z}$) have been fitted to a wide range of experimental data and those for H and He target atoms are shown in Figure 28. Three regimes of the parameter α can be identified and related to the collision velocity, namely:

$0.1 \leqslant \tilde{v} \leqslant 1$:- α is weakly dependent upon $\tilde{v}$ and it has a value close to unity.

$\tilde{v} > 1$:- α increases to an asymptotic value ($\alpha = 5$) when $\tilde{v} >> 1$.

$\tilde{v} \approx 2$ to 4 :- α becomes constant with a value close to 3.

The first of these regimes is the one most related to the plasma edge.

The preceding discussion has emphasised the role of ground state hydrogen atoms, but charge exchange may also involve excited

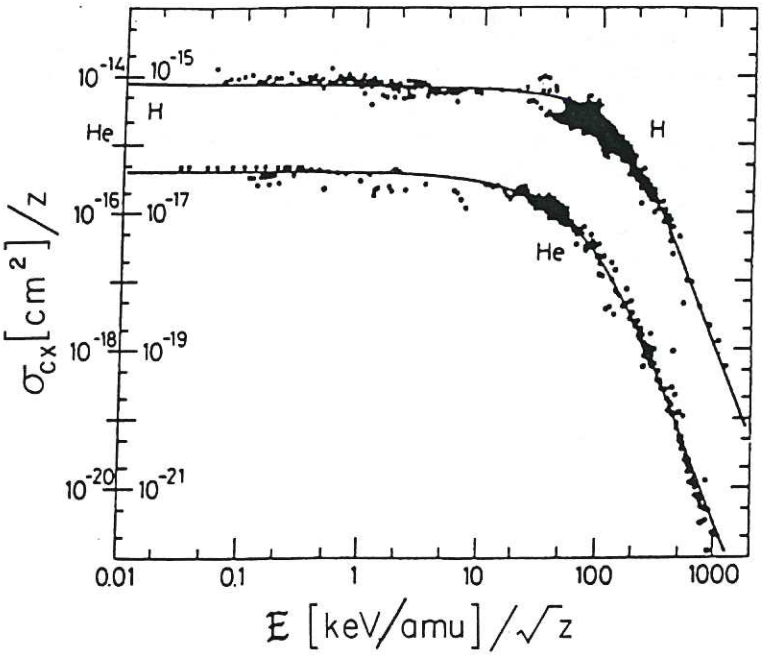

Fig. 28 Reduced electron capture cross section for ions with $z \geqslant 5$ in H and He atom targets.
Data taken from Janev and Hvelplund (Ref. 65).

H atoms. Cross sections[66] for charge exchange between $H(n) + He^{2+}$ are very large $\sim 10^{-12}$ cm^{-2} when $n > 8$ but such highly excited states of the hydrogen atom are unlikely to be strongly populated in the boundary plasma (see Section 10.1).

10. INFLUENCE OF THE PLASMA ENVIRONMENT

Application of basic cross section data must take account of the distribution of collision velocities within the plasma and also of the effects of multi-step collisions of the type discussed in Section 3.2. The possible presence of non-thermalised particles is neglected in order that the velocity distribution of plasma particles can be taken to be Maxwellian. The rate coefficient for an inelastic process with threshold energy E can then be calculated using

$$\langle \sigma v \rangle = \left(\frac{8k_B T}{\pi m}\right)^{1/2} \int_{E/k_B T}^{\infty} \sigma(\mathcal{E})\ (\mathcal{E}/k_B T) \exp(-\mathcal{E}/k_B T) d(\mathcal{E}/k_B T). \qquad (10.1)$$

The influence of this integral can be appreciated by comparing the electron impact ionisation cross section for H(1s) shown in Figure 12 with the corresponding ground state rate coefficient $S_i(g)$ shown in Figure 2. When $k_B T_e < E$ [say $\sim$ 2 eV for ionisation of H(1s) atoms] the form of the velocity distribution dominates the form of the rate coefficient so that uncertainty in the atomic cross section is of minor significance. However, when $k_B T \geq E$ the rate coefficient is sensitive to the cross section. It is useful when considering recycling of atomic hydrogen at boundary surfaces to note that, in a low temperature regime, the variation of the ionisation rate coefficient S_i with electron temperature is much greater than the possible variation of plasma parameters, e.g. $S_i(T_e)$ increases by a factor 10^4 over a temperature range $k_B T_e = 1$ to 10 eV. At moderate n_e, ionisation tends to take place near to the 5 eV isotherm.

10.1 Radiation Power Loses from Recycling Hydrogen

Electron collisions with hydrogen atoms and with protons give rise to radiative power losses as a consequence of the various reactions discussed in Section 3.2. The balance between these conflicting processes, which was first elucidated by Bates et al.[7], has been discussed in a number of papers, notably Bates and Kingston[67], McWhirter and Hearn[68] and Hutcheon and McWhirter[69]. Its relevance to the boundary plasma has been considered by Harrison[2,3] and by Janev et al[8]. Ionisation occurs either by a direct transition of the bound electron to the continuum (reaction 1, Section 3.2) or as the consequence of a sequence of transitions between excited levels (reaction 2) which terminates at the

continuum. The likelihood of the latter route depends upon the balance between the lifetime t_n of the excited states and the associated electron collision times

$$t_{en} = (n_e < \sigma_n v_e >)^{-1}. \qquad (10.2)$$

The lifetime of the state increases with increasing principle quantum number n and so does the collision cross section (i.e. $\sigma_n \propto n^4$) so that the multi-step route to ionisation becomes dominant for all but the lowest n states when $n_e \sim 10^{14}/cm^3$ or larger. In addition to the excited state n being destroyed by either an upward transition or direct ionisation it can also be destroyed by a downward, super-elastic collision (reaction 4). In effect the ability of the excited atom to radiate is reduced in favour of (i) ionisation by a chain of non-radiative upward transitions and (ii) by a complementary chain of non-radiative downward transitions which populate the ground state of the atom. In the limit of low electron density ($n_e \sim 10^{10}/cm^3$), the collision time t_{en} is much smaller than t_n so that the effects of multi-step processes can be neglected but, at higher density ($n_e \sim 10^{16}/cm^3$) most of the radiation is suppressed. It is convenient to express the volume rate for production of protons in the form

$$\nu_{H^+} = n_e \left[n_o(g)\, S_{CR} - n_i \alpha_{CR,H} \right]. \qquad (10.3)$$

Here the collisional radiative coefficients are composites of several components which account for the multi-step routes; $S_{CR}(T_e)$ for ionisation and $\alpha_{CR,H}(T_e)$ for electron-proton recombination. Both two body radiative processes (reaction 6) and three body processes (reaction 7) must be included, i.e.

$$\alpha_{CR,H}(T_e) = [\alpha(\text{two-body}) + \alpha(\text{three-body})]. \qquad (10.4)$$

The ion recombination time

$$t_\alpha = (n_e\, \alpha_{CR,H})^{-1} \qquad (10.5)$$

is generally smaller than the proton residence time in the boundary plasma so that recombination tends to be insignificant. In contrast, the electron-atom collision times t_{en} are sufficiently short for a quasi-steady state population of excited levels to be established by multi-step processes. In such conditions the average energy required to produce one proton-electron pair (E_{ion}) can be considered in a collective manner as the amount of energy expended in ionisation plus the amount radiated from the small number of low lying excited states which are not depopulated by multi-step processes. Following the approach of McWhirter and Hearn[68], this energy can be expressed as

$$E_{ion} = \frac{(E_i S_{CR} + P_l \, n_e^{-1})}{S_{CR}} \qquad (10.6)$$

where P_l is the coefficient for line radiation losses defined in relation to the density of ground state atoms [in a manner analogous to that indicated in Eq. (10.15)]. Estimated values of E_{ion} which are shown in Figure 29 are taken from a calculation by McWhirter and Hearn which relates to hydrogenic ions (e.g. He^+, Li^{2+} etc.) so that the plasma parameters can be scaled with atomic number Z in the following manner:

$$[T_e]_Z \equiv Z^2[T_e]_H; \; [E_{ion}]_Z \equiv Z^2[E_{ion}]_H \text{ and } [n_e]_Z \equiv Z^{-7}[n_e]_H.$$

The plotted data are for the equivalent hydrogen "atom" and so correspond to Z = 1. These authors employ Coulomb Born ionisation cross sections for the determination of S_{CR} but the Coulomb acceleration causes such calculations to overestimate the ionisation cross section of the hydrogen atom at low electron energy (as can be seen in Figure 13). The extent of this overestimation can be seen by comparison with the data points in Figure 29 which refer specifically to hydrogen atoms. More recent detailed calculations for hydrogen atoms by

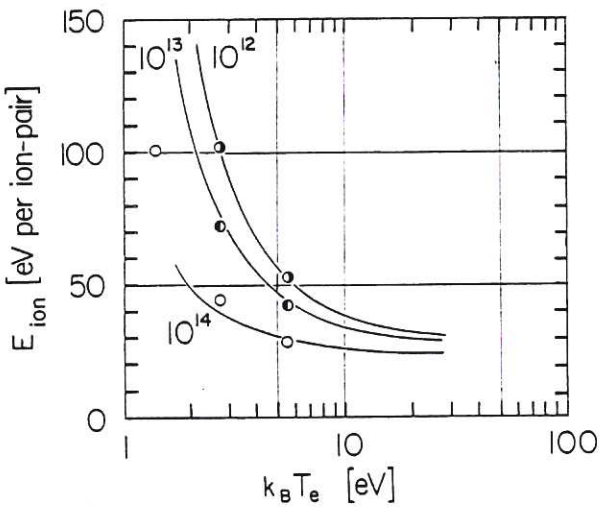

Fig.29 The average energy require to produce one electron-proton pair in atomic hydrogen.
Solid lines are data for hydrogenic ions taken from McWhirter and Hearn[69] and the circles show the data for hydrogen atoms (taken from Bates et al.[7] and Bates and Kingston (Ref. 67).

Janev et al.[8] are in close agreement with these data. In this collective concept, the amount of radiated energy associated with each ionisation event is given by

$$E_H^{rad} = E_{ion} - 13.6 \quad [eV]. \qquad (10.7)$$

It is worthwhile noting the Z dependence of the scaling relationships which imply that multi-step processes for He^+ are of but slight significance in the boundary plasma where n_e is unlikely to exceed a few $10^{14}/cm^3$.

The influence of the confining magnetic field upon the excited state population has been neglected in the preceding discussion. Its effects are two-fold. Firstly there are Lorentz forces $[e(\vec{B} \times \vec{v})]$ exerted upon the bound electron due to atom motion across the magnetic field and the associated electric field can destroy the higher n levels by field ionisation. Ionisation of highly excited Rydberg states by electric fields is discussed in detail by Brouillard[70]. Janev et al.[8] estimate for typical boundary plasma conditions that Lorentz forces lower the ionisation continuum so that it coincides with an n value of about 26. Such lowering of the ionisation continuum by Lorentz forces, and also by electric fields which arise due to statistical deviation from local charge neutrality of the plasma, are in practice insignificant because the destruction rate of these high n states by electron collisions is very large indeed. Secondly the presence of the magnetic field causes the atomic levels to be split due to the Zeeman effect (which is described, for example, in Ref. 9) so that neighbouring states become mixed. Stark splitting, which arises due to electric fields (such as the Lorentz field) also causes level mixing. In the particular case of atomic hydrogen such mixing dramatically reduces the lifetime of the metastable $2^2S_{\frac{1}{2}}$ state which mixes readily with the short lived $2^2P_{\frac{1}{2}}$ state (for a detailed discussion of the spectra of the H atom see Ref. 71). Consequently the effects of metastable atoms can be ignored. This does not conflict with the preceding calculations which account only for the principal n levels and thereby neglect contributions from sub-levels.

10.2 Charge State Distribution of Impurity Ions and Radiative Power Losses

The treatment of impurity species follows along similar lines to that described for hydrogen atoms and hydrogenic ions but it is more complicated due to the complex nature of the electron configuration of these atomic species. It is in general reasonable to accept that ionisation by electron collisions proceeds in a stepwise manner, i.e. $X^o \rightarrow X^+ \rightarrow X^{2+} \longrightarrow$ etc., so that the steady state balance of an ionisation stage z can be expressed as

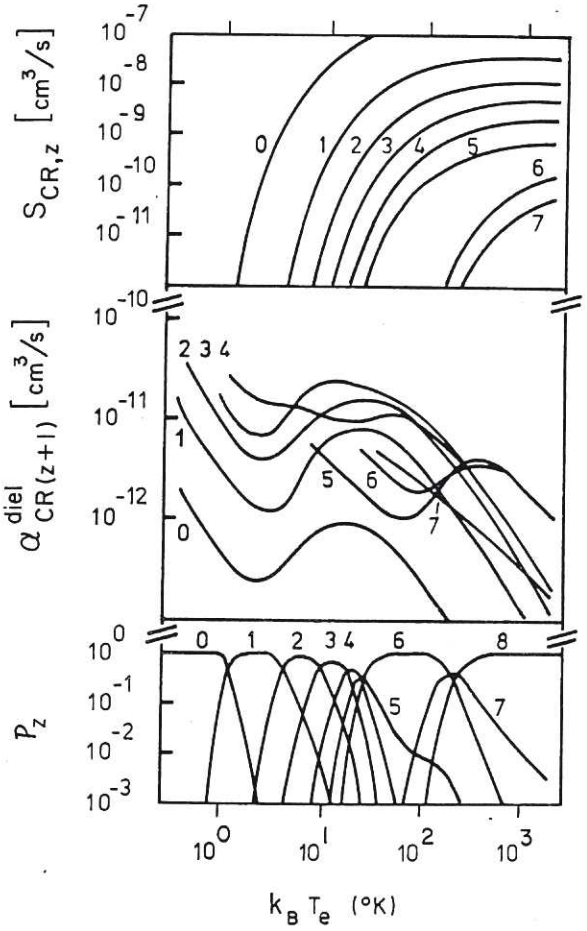

Fig. 30 Collisional radiative rates for ionisation, $S_{CR,z}(T_e)$, dielectronic recombination $\alpha^{diel}_{CR(z+1)}(T_e)$ together with the charge state population (P_z) for oxygen.
Data which are taken from Summers[73] are for $n_e = 10^{12}/cm^3$.
The ion charge state z is shown for each curve.

$$n_e n_{(z-1)} S_{CR(z-1)} - n_e n_z S_{CR,z} + n_e n_{(z+1)} \alpha_{CR(z+1)} - n_e n_z \alpha_{CR,z} - n_z/\tau_z = 0. \qquad (10.8)$$

Here the ion density (n_z etc.) refers to the ground state and any contribution from the population of excited states are accommodated by the use of appropriate collisional radiative coefficients. Details of the physics involved and of the modelling employed in determining these coefficients can be found in McWhirter and Summers[6] and also in Drawin[72]. Dielectronic recombination (reaction 12) provides a powerful route for recombination of these multi-electron species and so the various contributions to recombination

$$\alpha_{CR,z} = [\alpha(\text{two body radiative}) + \alpha(\text{dielectronic}) + \alpha(\text{three body})] \qquad (10.9)$$

must be included.

The time τ_z in Eq. (10.8) is the residence time of the ions in the particular plasma region under consideration. If this region is sited deeply within the closed confinement field of the plasma then

$$\tau_z \gg [n_e \alpha_z(T_e)]^{-1} \qquad (10.10)$$

and the charge state density population tends to be in equilibrium. It is then governed by the electron collision rates so that

$$\frac{n_{(z+1)}}{n_z} = \frac{S_{CR,z}(T_e)}{\alpha_{CR(z+1)}(T_e)}. \qquad (10.11)$$

This is the condition of "local thermal equilibrium" which is often referred to as "coronal equilibrium" and its characteristics are illustrated for the example of oxygen in Figure 30. It should be noted that the population ($P_z = n_z/\Sigma n_z$) of the charge state z is substantial when $S_{CR,z}(T_e) = \alpha_{CR(z+1)}(T_e)$ and that this equality occurs in the regime where $k_B T_e < E_{i,z}$. Thus the population of ionisation stages tends to be sensitive to the low temperature regime of the ionisation rate coefficient.

If the plasma region under consideration lies close to the edge or if the effective drift velocity of the atomic particles is large (one such example arises when substantial numbers of energetic atoms are injected) then the inequality expressed in Eq. (10.10) is no longer valid and the ion loss rate in Eq. (10.8) becomes dominant. These "non-coronal" conditions are particularly evident in the open magnetic field region of the plasma edge because here ions are lost from the system due to rapid transport along the field to the boundary surfaces so that the effects of recombination are substantially reduced. It is convenient to simplify Eq. (10.8) by assuming that the residence time of impurity ions is insensitive to their charge state (i.e. $\tau_z = \tau_{imp}$) and the results of one such calculation for oxygen by Abramov[74] are shown in Figure 31. Here the average charge state

$$\bar{z} = \frac{\Sigma z n_z}{\Sigma n_z} \qquad (10.12)$$

is plotted as a function of $k_B T_e$ for various values of $n_e \tau_{imp}$; typically $n_e \tau_{imp} \sim 5 \times 10^{10}$ $cm^{-3}s$ in the boundary plasma.

Estimation of τ_z or τ_{imp} requires a detailed knowledge of plasma transport in the edge plasma. Neuhauser et al.[75] have

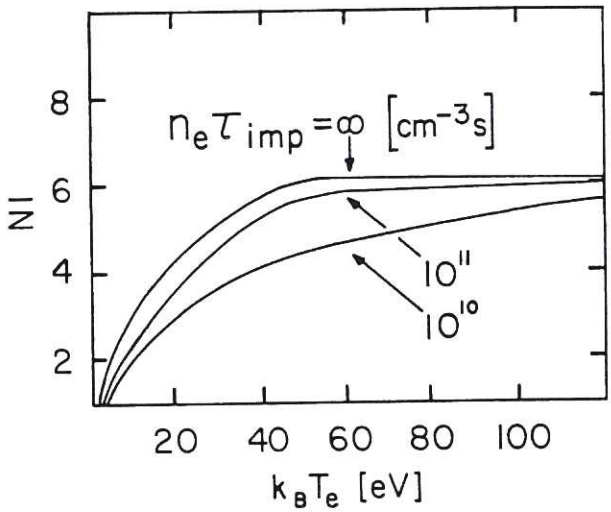

Fig. 31 The average charge state $\bar{z}$ of oxygen plotted as a function of electron temperature.
Data are taken from Abramov[74] and the condition $n_e\tau_{imp} = \infty$ is equivlent to the coronal equilibrium conditions shown in Figure 30.

evolved both one dimensional and quasi-two dimensional models for impurity ion transport parallel to the magnetic field within the drifting hydrogen plasma of the scrape-off and divertor region of a tokamak. They find that the peak of the charge state distribution is likely to occur at $z \sim 2$ to 3 when most impurity ionisation occurs within the high recycling region close to the divertor target. A similar conclusion is reached by Harrison[2,3] but his approach is based upon a much simpler concept; recombination is neglected and τ_{imp} set equal to the thermalisation time of the impurity ions within the drifting background hydrogen plasma. It must be stressed that such low charge states are attained solely by impurities which recycle in the immediate vicinity of a divertor target (or limiter). The residence time of ions which originate from the bulk of the first wall can be quite long because of the low flow velocity within the scrape-off plasma when high recycling occurs at a divertor target. In such cases $z \sim 10$ may be encountered for medium and high z ions.

Contributions to the balance of ionisation states of impurities due to charge capture from H atoms is to be expected whenever the local density of atomic hydrogen is significant and the charge state of impurity ions moderately high. A discussion of the likely significance of such effects can be found in Drawin[1]. Hydrogen atom density can be high in the recycling region adjacent to boundary surfaces but here the average charge state of impurities is insufficient for charge exchange to contribute substantially. In general, the effects of charge exchange are

only likely to impact upon the ionisation stage population when fast atoms are injected into the plasma.

The population of excited states reaches a steady state value in a much shorter time than does the charge stage distribution. The equilibrium balance of excited states can be conveniently expressed in the form

$$\frac{n_{zq}}{n_{zo}} = \frac{n_e \, S^{CR}_{oq}}{\sum_{p<q} A_{(q\to p)}} \qquad (10.13)$$

where n_{zq} is the density of ions (of charge stage z) in excited level q, n_{zo} is the density of groundstate ions, S^{CR}_{oq} is the collisional radiative excitation coefficient for transitions $0 \to q$ and $(A_{q\to p})^{-1}$ is the lifetime for spontaneous decay from q to a lower level p. The density of power radiated due to the spontaneous decay of level q to p is

$$P_{z(q\to p)} = n_{zq} \, A_{(q\to p)} \, E_{pq} \qquad [1.6 \times 10^{-19} \text{W/cm}^3]. \qquad (10.14)$$

The power loss due to line radiation from ionisation stage z

$$P_{zl}(T_e) = \sum_q P_{z(q\to p)}(T_e) \qquad (10.15)$$

is determined by summation over those q levels which (a) have a significant excitation rate coefficient, (b) are not depopulated by multi-step processes and (c) emit photons which carry a significant amount of energy. Details of modelling methods can be found in McWhirter and Summers Ref. 6. As would be expected from the discussion of excitation given in Section 8, the summation in Eq. (10.15) tends to be dominated by transitions in which $\Delta n = 0$.

The total power loss $P_{zt}(T_e)$ due to radiation associated with charge state z must also include contributions from recombination which are of the form

$$P_{\alpha z} \sim n_e \, n_z \, \alpha_{CR,z}(T_e) \, \Delta E \qquad (10.16)$$

where ΔE is the total amount of kinetic energy lost by the plasma electron. These power loss components can be grouped in the following manner

$$P_{tz}(T_e) = [P_l(T_e) + P_\alpha(T_e) + P_{br}(T_e)]_z = n_e \, n_z \, F_z(T_e) \qquad (10.17)$$

so that the radiated power function

$$F_z(T_e) = P_{tz}(T_e)/n_e \, n_z \qquad [\text{W cm}^3] \qquad (10.18)$$

can be used as a measure of the radiating efficiency of each ionisation stage z. Summation of $F_z(T_e)$ over the population of ionisation stages yields the radiated power loss coefficient $F = P(T_e)/n_e n_{imp}$ which is characteristic of the particular atomic species. The radiated power loss functions for the coronal equilibrium charge state distributions of oxygen (shown in Figure 30) are of the form shown in Figure 32.

The total radiated power function can be strongly sensitive to deviation of plasma conditions away from those of local thermal equilibrium. This effect can be seen in Figure 33 where $P/n_e n_{imp}$, for various values of $n_e \tau_{imp}$, is plotted as a function of $k_B T_e$ (the associated average charge states are presented in Figure 31). A marked sensitivity of the total radiation function to $n_e \tau_{imp}$ is evident when $k_B T_e$ exceeds 30 eV.

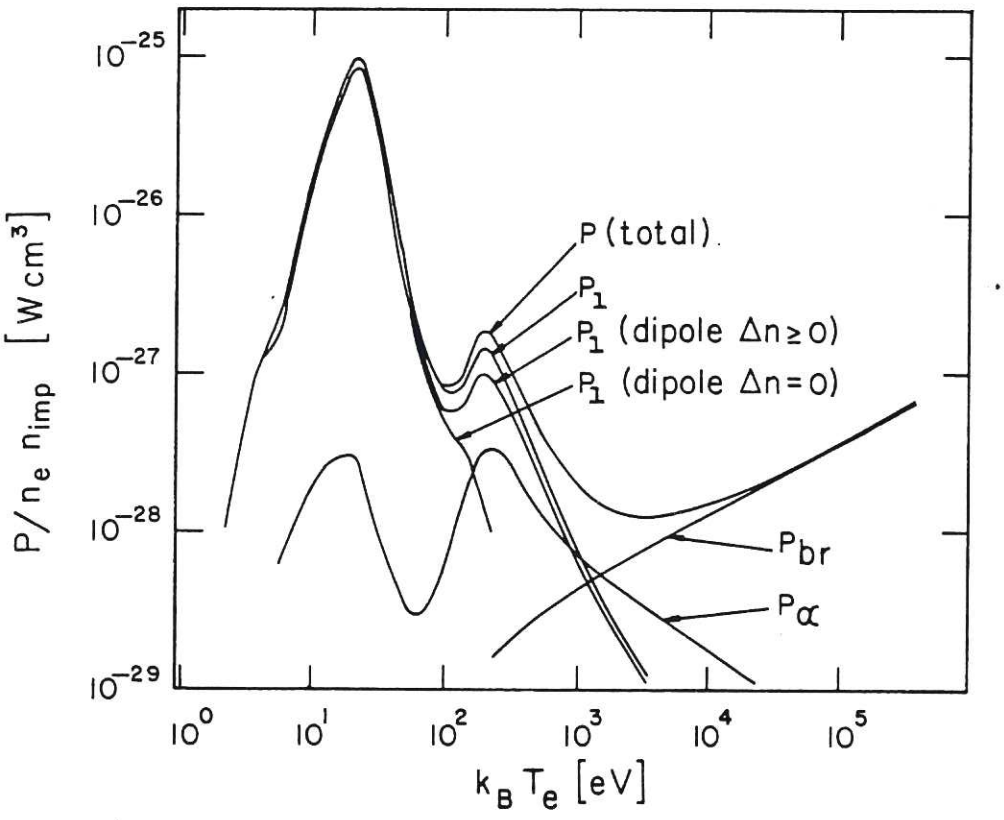

Fig. 32 Radiated power loss function for oxygen. Data are taken from Summers and McWhirter[76]. Individual contributions from line radiation, recombination radiation and bremsstrahlung radiation are shown. The component due to line radiation is further resolved into contributions from dipole transitions where $\Delta n \geq 0$ and where $\Delta n = 0$.

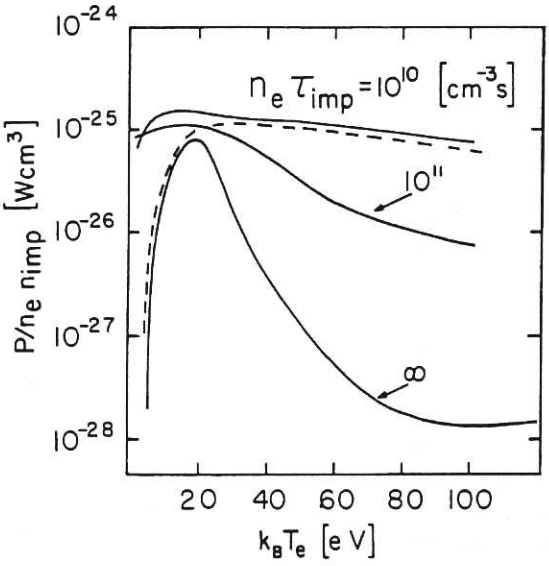

Fig. 33 Total radiated power loss functions for oxygen. Solid curves are the data of Abramov[74] and apply to the average charge states shown in Figure 31. The dashed curve is the data of Shimada et al. (Ref. 77). Note coronal equilibrium conditions correspond to $n_e \tau_{imp} = \infty$.

Detailed calculations along the lines described by Summers and McWhirter (and shown here in Figure 32) yield the best available data for radiative power losses but the procedure is both complex and time consuming. Such data are therefore restricted to a relatively small number of atomic species. Furthermore, the collision data for neutral and lowly charged complex atomic species such as iron and tungsten are so uncertain that such precise calculation of their power losses is not warranted at low plasma temperatures. Jensen et al.[78] have invoked the concept of an "average ion" model in order to simplify calculation of radiative power losses and thereby provide a wider base of data. The different ion charge states of each atomic species are replaced by a single conceptual "average ion". The populations of the ionisation stages in the real plasma are statistically accounted for by assigning equivalent electron populations to the principle electron shells of the average ion. Transitions between these levels are equivalent to changes in ionisation stage. Radiative power losses are related to transitions between the electron levels of this average ion. A wide range of data based upon this method has been reported by Post et al[79].

11. CONCLUSION

Although the preceding discussion has emphasised the physical properties of atomic and molecular collisions within the edge region it is obvious that these basic properties are valid throughout the bulk of the confined plasma. Nevertheless, the significance of a particular process is dependent upon the local plasma environment. In the hotter central region, the ion residence times are relatively long so that (a) impurity ions can be raised to much higher charge states and (b) recombination plays a powerful role in determining the population of ionisation states. In contrast, molecular processes become insignificant. Electron-proton recombination exercises a negligible effect upon the bulk plasma and charge capture due to collisions between impurity ions and hydrogen atoms become significant only if the atoms can penetrate the plasma. Typical examples are energetic neutral beams used for heating or diagnostics. Such energetic hydrogen atoms are confined within the plasma when they become ionised mainly by collisions with plasma protons. Both charge exchange and direct ionisation contribute but at high atom energies ($E > 50$ keV for H atoms) trapping due to proton impact ionisation has the most pronounced effect. Cross sections for double electron capture become quite large at very high energies (a few 100 keV/amu) and so fusion α-particles can partake in such interactions. In addition to collision processes which directly influence plasma conditions within the bulk and edge regions there are many other processes which impact upon diagnostic studies and upon the peripheral technological requirements of fusion devices. A typical example is the generation of intense beams of energetic atoms. Recent reviews of these broader issues can be found in Drawin[80], Post[81] and Harrison[82] and beam formation is reviewed by Green in Ref. 83.

The status of available data relevant to the edge plasma reflects the balance between the present limitations of theory and experiment. In the case of cross sections for electron ionisation and excitation of atomic hydrogen there is a good base of measured data and extrapolation by precise theoretical treatment is feasible for this simplest atomic system. Measurements of H atom charge transfer (and ionisation) in collisions with protons are plentiful and extend over a wide range of energy (from 1 eV to several MeV). Measured data for charge exchange between H atoms and impurity ions are rather sparse and limited to relatively low charge states (typically $z < 10$). Theoretical treatment and scaling of charge exchange is uncertain at low energies and low charge states. There are very few experimental studies of collisions between protons and impurity ions and the data do not extend below proton energies of $\sim$ 1 keV; theoretical treatment of these collisions is uncertain. Measured cross section data for electron impact ionisation of atoms and ions of low atomic number elements is plentiful (at least for charge states less than $z = 5$), so that extrapolation can be under-

taken with a fair degree of confidence (see Ref. 40). There are but a few measured ionisation cross sections for atoms and ions of heavier elements and theoretical treatment is uncertain for the lowly charged ions of complex atomic species; for lack of better data, semi-empirical cross sections have perforce to be employed. Apart from those atoms which can be studied in gas cell experiments, there are virtually no measured data for electron impact excitation cross sections of relevant atoms and ions. The main experimental problems are associated with the precise detection of energy resolved photons in colliding beam experiments (see the brief discussions in Section 6.3). This problem can, in principle, be avoided by detecting the inelastically scattered electrons rather than the photons. This solution has long been appreciated (see comments by Harrison[84] and Dunn[33]) but such experiments are difficult and the first such study (for Zn^+) was reported by Chutjion and Newall[85] as late as 1982. In the case of electron collisions with neutral H_2 molecules (see the review by de Heer[39]) there is a fair amount of measured data for the production of radiation and also of charged particles but the cross section for dissociation of H_2 into two ground state H atoms remains uncertain. Fast colliding beam experiments (reviewed by Dolder and Peart[86]) have provided a sound base of data for electron collisions with H_2^+ ions.

Recombination becomes increasingly important as the region under consideration is sited more deeply within the confined plasma. Concise reviews of experimental methods used to study both radiative and dielectronic recombination under single collision conditions can be found in Refs. 86, 31 and 33 . Unfortunately such methods do not yet yield data for multiply charged impurity ions and so the present results are not directly applicable. Studies of moderately intense plasmas can of course, when precisely interpreted, yield data for the rate coefficients involved in, ionisation, excitation and recombination. The techniques are reviewed by Kunze[87] and measurements of excitation rates are discussed by Gabriel and Jordan[88].

In addition to the valuable review articles that emerge from the academic community the fusion researcher is also served by a number of data centres wherein data are assessed and compiled. Notable amongst these centres are the Oak Ridge National Laboratory and the Bureau of Standards in the USA, the Institute of Plasma Physics (Nagoya University, Japan), the Kurchatov Institute (Moscow, USSR) and Queen's University (Belfast, UK). The International Atomic Energy Agency (Vienna, Austria) provides an international service in close collaboration with the fusion data centres. The I.A.E.A. publishes a quarterly "International Bulletin on Atomic and Molecular Data for Fusion" which contains up to date indexes of the relevant literature. A comprehensive index of literature up to 1979 can be found in CIAMDA 80 (Ref. 89). Assessment of the validity of data is a difficult and somewhat subjective task calling for the

balanced opinions of both theorists and experimentalists. Specialist workshops are organised by the I.A.E.A. and these recommend (Ref. 90) the best available data.

REFERENCES

1. H.W. Drawin, Atomic and Molecular Processes in High-Temperature, Low-Density Magnetically Confined Plasmas, in Ref. 17, p.341.
2. M.F.A. Harrison, The Plasma Boundary and the Role of Atomic and Molecular Processes, in Ref. 17, p.441.
3. M.F.A. Harrison, Boundary Plasma, in Ref. 19, Vol. 2, p.395.
4. W. Grotian "Graphische Darstellung der Spektren von Atomen und Ionen mit zwei und drei Valenzelektronen", Springer, Berlin (1928).
5. K. Takayanagi and H. Suzuki, "Cross Sections for Atomic Processes, Vol.1. Processes involving Hydrogen Isotopes, their ions, electrons and photons", English version of Report IPPJ-DT-48, Nagoya University, Institute of Plasma Physics, Nagoya (1978).
6. R.P. McWhirter and H.P. Summers, Atomic Radiation from Low Density Plasma, Ref.19, Vol.2, p.52.
7. D.R. Bates, A. Kingston and R.W. McWhirter, Proc. Roy. Soc. A267, 297, 1962.
8. R.K. Janev, D.E. Post, W.D. Langer, K. Evans, D.B. Heifetz and J.C. Weisheit, J.Nucl.Mater. 121: 10,(1984).
9. G. Herzberg, "Atomic Spectra and Atomic Structure", Dover Publications, New York (1944).
10. C. Candler, "Atomic Spectra and the Vector Model", Hilger and Watts, London (1964).
11. V.L. Jacobs, J. Davies, J.E. Rogerson and M. Blaha, Astrophys. J.230: 627 (1979).
12. A.G. Gaydon, "Dissociation Energies and Spectra of Diatomic Molecules", Chapman and Hall, London (1953).
13. C.F. Barnett, J.A. Ray and J.C. Thompson, "Atomic and Molecular Collision Cross Sections of Interest in Controlled Thermonuclear Research", Report ORNL-3113 Oak Ridge National Laboratory, Oak Ridge (1964).
14. H.S.W. Massey, E.H.S. Burhop and H.B. Gilbody, "Electronic and Ionic Impact Phenomena", Vols. 1 to 5, Oxford University Press, Oxford (1974).
15. E.W. McDaniel, "Collision Phenomenon in Ionized Gases", John Wiley and Sons, New York (1964).
16. "Atomic and Molecular Processes in Controlled Thermonuclear Fusion" ed., M.R.C. McDowell and A.M. Ferendeci, NATO ASI, Bonas, France, Plenum Press, New York and London (1980).
17. "Atomic and Molecular Physics of Controlled Thermonuclear Fusion" ed., C.J. Joachain and D.E. Post, NATO ASI, Santa Flavia, Italy, Plenum Press, New York and London (1983).

18. "Physics of Ion-Ion and Electron-Ion Collisions, ed., F. Brouillard and J.W. McGowen, NATO ASI, Baddeck, Canada, Plenum Press, New York and London (1983).
19. "Applied Atomic Collision Physics" Vols. 1 to 5, ed., H.S.W. Massey, E.W. McDaniel and B. Bederson, Academic Press, New York and London (1983).
20. J. J. Thomson, Phil. Mag. 23: 419 (1912).
21. M. Born, Z. Physik, 38: 803 (1926).
22. H.A. Bethe, Ann. Physik, 5: 325 (1930).
23. C.J. Joachain, Theoretical Methods for Atomic Collisions - A General Survey, in Ref. 16, p.147 and Recent Progress in Theoretical Models of Atomic Collisions, in Ref. 17, p.139.
24. T. Kato, "Ionisation and Excitation of Ions by Electron Impact - Review of empirical formulae", Report IPPJ-AM-2, Nagoya University, Institute of Plasma Physics, Nagoya (1978).
25. Y. Itikawa and T. Kato, "Empirical formulas for Ionisation Cross Section of Atomic Ions for Electron Collisions", Report IPPJ-AM-17, Nagoya University, Institute for Plasma Physics, Nagoya (1981).
26. W. Lotz, Z. Phys. 220: 466 (1969).
27. H. van Regemorter, Astrophys. J. 136: 906 (1962).
28. A. Burgess, Mem. Soc. Roy. Sci. Liege, 4: 299 (1961).
29. M.J. Seaton, Excitation and Ionisation by Electron Impact, p.375, in "Atomic and Molecular Processes" ed., D.R. Bates, Academic Press, New York (1962).
30. J.A. Gaunt, Phil. Trans. A229: 163 (1930).
31. D.H. Crandall, Electron Ion Collisions, in "Atomic Physics of Highly Ionised Atoms", ed. R. Marrus, NATO ASI, Cargese, Corsica, France, Plenum Press, New York and London (1982) also Report ORNL/TM-8453, Oak Ridge National Laboratory, Oak Ridge (1982).
32. D.H. Crandall, Electron Impact Excitation of Ions, in Ref. 13, p.201.
33. G.H. Dunn, Electron Ion Collisions in "Physics of Ionised Gases", ed., H. Matie and B. Kidric, Inst. Nucl. Science, Belgrade (1980).
34. K.T. Dolder, Experimental Aspects of Electron Impact Ionisation and Excitation of Positive Ions, in Ref. 17, p.213.
35. W.L. Fite and R.T. Brackman, Phys. Rev. 112: 1141 (1958).
36. K.T. Dolder, M.F.A. Harrison and P.C. Thonemann, Proc. Roy. Soc. A 264: 367 (1961).
37. M.F.A. Harrison, Colliding Beam Studies of Atomic Collision Processes, in "Low-energy Ion Beams", p.190, ed. K.G. Stephens, I.H. Wilson and J.L. Moruzzi, Inst. Phys. Conf. Ser. No.38 (1978).
38. L.J. Kieffer and G.H. Dunn, Rev. Mod. Phys. 38: 1 (1966).
39. F.J. De Heer, Experiments on Electron Capture and Ionisation by Ions, in Ref. 16, p.351 and Experiments on Electron Capture and Ionisation by Multiply Charged Ions, in Ref.17, p.269.

40 K.L. Bell, H.B. Gilbody, J.G. Hughes, A.E. Kingston and F.J. Smith, "Recommended Cross Sections and Rates for Electron Ionisation of Light Atoms and Ions", Report CLM-R216, Culham Laboratory, Culham (1982).
41. P. Defrance, W. Claeys, A. Cornet and G. Poulaert, J.Phys.B: Atom. Molec. Phys. 14: 111 (1981).
42. R.G. Montague, M.J. Diserens and M.F.A. Harrison, J. Phys. B. 17: 2085 (1984).
43. J. McGuire, Phys. Rev. A 16: 73 (1977).
44. C.F. Barnett, J.A. Ray, E. Ricci, M.I. Wilker, E.W. McDaniel, E.W. Thomas and H.B. Gilbody, "Atomic Data for Controlled Fusion Research". Reports ORNL-5260 (Vol. 1) and ORNL-5207 (Vol. 2), Oak Ridge National Laboratory, Oak Ridge (1977).
45. D.F. Dance, M.F.A. Harrison and A.C.H. Smith, Proc. Roy. Soc. A290: 74 (1966).
46. A. Burgess and M.C. Chidichimo, Mon. Not. R.A.S. 203: 1269 (1983).
47. D.F. Dance, M.F.A. Harrison, R.D. Rundel and A.C.H. Smith, Proc. Phys. Soc. 92: 577 (1967).
48. G.H. Dunn, J. Chem. Phys. 44: 2592 (1966).
49. F.J. de Heer, Physica Scripta, 23: 170 (1981).
50. B.H. Bransden, Theoretical Models for Charge Exchange, in Ref. 16, p.185 and The Theory of Charge Exchange and Ionistion by Heavy Particles, in Ref. 17, p.245.
51. R.K. Janev and B.H. Bransden, "Charge Exchange between Highly Charged Ions and Atomic Hydrogen: A Critical Review of Theoretical Data", Report INDC (NDS)-135/GA, IAEA, Vienna (1982).
52. H.B. Gilbody, Physica Scripta, 24,: 712 (1981).
53. H.S.W. Massey, Rep. Prog. Phys. 12: 248 (1949).
54. J.B. Hasted in "Advances in Eectronics and Electron Physics" Vol. XIII, p.1, ed. L. Morton, Academic Press, New York (1960).
55. R.E. Olson, A. Salop, P.A. Phaneuf and F.W. Meyer, Phys. Rev. A16: 1867 (1977).
56. P. Hvelplund and A. Andersen, Physica Scripta, 26: 370 (1982).
57. J.H. Newman, J.D. Cogan, D.L. Ziegler, D.E. Nitz, R.D. Rundel, K.A. Smith, R.F. Stebbings, Phys. Rev. A25: 2976 (1982).
58. P.T. Greenland, "Low Energy Charge Capture Cross Sections", Report AERE-R11282, Atomic Energy Research Establishment, Harwell (1984).
59. W.L. Fite, A.C.H. Smith and R.F. Stebbings, Proc. Roy. Soc. A268: 527 (1963).
60. R.F. Stebbings, A.C.H. Smith and H. Ehrhardt, in "Atomic Collision Processes", p.814, ed. M.R.C. McDowell, North Holland, Amsterdam (1964).
61. G. Herzberg, "Molecular Spectra and Molecular Structure, I. Spectra of Diatomic Molecules", D. van Nostrand Co. Inc. Princeton (1950).
62. L. Landau, Z. Phys. Sowjet 2: 46 (1932) and C. Zener, Proc. Roy. Soc. A137: 696 (1932).

63. D.A. Hobbis, P. Nickolson, M.F.A. Harrison and R.G. Montague, to be submitted to J. Phys. B.
64. A. Salop and R.E. Olson, Phys. Rev. A13: 1312 (1976).
65. R.K. Janev and P. Hevelplund, Comments in Atomic and Molecular Physics, XI, 75 (1981).
66. M. Buriaux, F. Brouillard, A. Joynaux, T. Govers and S. Szücs, J. Phys. B. 10: 2421 (1977).
67. D.R. Bates and A.E. Kingston, Planet and Space Science, 11: 1 (1963).
68. R.W.P. McWhirter and A.G. Hearn, Proc. Phys. Soc. 82: 641 (1963).
69. R.J. Hutchinson and R.W.P. McWhirter, J. Phys. B. 6: 2668 (1973).
70. F. Brouillard, Rydberg States, in Ref. 17, p.313.
71. G.W. Series, "The Spectrum of Atomic Hydrogen", Oxford University Press, Oxford (1957).
72. H.W. Drawin, Phys. Rep. 37: 125 (1978).
73. H.P. Summers, "Tables and Graphs of Collisional Dielectronic Recombination and Ionisation Coefficients and Ionisation Equilibria of H-like to A-like Ions of Elements", Appleton Laboratory Memo. IM 367, Appleton Laboratory, Culham (1974).
74. V.A. Abramov, in "USSR Contributions to the INTOR Phase-Two-A Workshop", Report, Kurchatov Institute, Moscow (1982) also "International Tokamak Reactor: Phase-Two-A", p.215, International Atomic Energy Agency, Vienna (1983).
75. J. Neuhauser, W. Schneider, R. Wunderlich and K. Lackner, J. Nucl. Mater. 121: 195 (1984).
76. H.P. Summers and R.W.P. McWhirter, J. Phys. B. 12: 2387 (1979).
77. M. Shimada, M. Nagami, K. Ioki, S. Izumi, M. Maeno, H. Yokomizo, K. Shinya, H. Yoshida, N.H. Brooks, C.L. Hsieh, A. Kitsunezaki and N. Fujisawa, in "Japanese contribution to the INTOR Phase-Two-A Workshop", Japan Atomic Energy Research Institute, Tokai-mura (1982).
78. R.V. Jensen, D.E. Post, W.H. Grasberger, C.B. Tarter and W.A. Lokke, Nucl. Fusion, 17: 1187 (1977).
79. D.E. Post, R.V. Jensen, C.B. Tarter, W.H. Grasberger and W.A. Lokke, At. Data and Nuc. Data Tables, 20: 397 (1977).
80. H.W. Drawin, Physica Scripta, 24: 622 (1981).
81. D.E. Post, The Role of Atomic Collisions in Fusion, in Ref. 18, p.37.
82. M.F.A. Harrison, The Relevance of Atomic Processes to Magnetic Confinement and the Concept of a Tokamak Reactor, in Ref. 16, p.15.
83. T.S. Green, Neutral Beam Formation and Transport, in Ref. 19, Vol. 2, p.339.
84. M.F.A. Harrison, Electron Impact Ionisation and Excitation of Positive Ions, in "Methods in Experimental Physics", Vol. 7B, p. 95, ed. W.L. Fite and B. Bederson, Academic Press, New York (1968).

85. A. Chutjian and W.R. Newall, Phys. Rev. A26: 2271 (1982).
86. K.T. Dolder and B. Peart, Rep. Prog. Phys. 39: 697 (1976).
87. H.J. Kunze, Space Sci. Rev. 13: 565 (1972).
88. A.H. Gabriel and C. Jordan, in "Case Studies in Atomic Collision Physics II", p.209, ed. E.W. McDaniel and M.R.C. McDowell, North-Holland Publishing Co., Amsterdam (1972).
89. CIAMDA 80, "An Index to the Literature of Atomic and Molecular Collision Data Relevant to Fusion Reseach, International Atomic Energy Agency, Vienna, Austria (1980).
90. "Research Coordination Meetings on Atomic Collision Data for Diagnostics of Magnetic Fusion Plasmas":
First Meeting: IAEA Report, INDC(NDS)-136/GA (1982).
Second Meeting: IAEA Report, INDC(NDS)-150/GA (1984).
Third Meeting: IAEA Report, INDC(NDS)-160/GA (1984).